MAGNETO-OPTICAL IMAGING OF FLUX PENETRATION IN HIGH TEMPERATURE SUPERCONDUCTING THIN FILMS

by

Per H. Brown

THESIS SUBMITTED IN PARTIAL FULFILLMENT OF

THE REQUIREMENTS FOR THE DEGREE OF

MASTER OF SCIENCE

in the Department

of

Physics

SIMON FRASER UNIVERSITY

March 1994

APPROVAL

Name : Per H. Brown

Degree : Master of Science

Title of thesis : Magneto-Optical Imaging of Flux Penetration in High Temperature Superconducting Thin Films

Examining Committee :

Chairman : M. Thewalt

J.C. Irwin

Senior Supervisor

B. Heinrich

A. Curzon

S. Gygax

Date Approved : March 11, 1994

PARTIAL COPYRIGHT LICENSE

I hereby grant to Simon Fraser University the right to lend my thesis, project or extended essay (the title of which is shown below) to users of the Simon Fraser University Library, and to make partial or single copies only for such users or in response to a request from the library of any other university, or other educational institution, on its own behalf or for one of its users. I further agree that permission for multiple copying of this work for scholarly purposes may be granted by me or the Dean of Graduate Studies. It is understood that copying or publication of this work for financial gain shall not be allowed without my written permission.

Title of Thesis/Project/Extended Essay

Magnetic-Optical Imaging of Flux Penetration in High Temperature Superconducting Thin Films.

Author: _____

(signature)

Per Brown

(name)

March 15/94

(date)

Abstract

The magnetic properties of the high temperature superconductors $YBa_2Cu_3O_{7-x}$ and $Tl_2Ba_2CaCu_2O_8$ have been investigated using a magneto-optical technique. Thin superconducting films of the samples were grown by laser ablation by a local company called CTF Systems Inc. A garnet film was placed above the surface of the superconducting film and the domain structure in the film was thus sensitive to variations of any magnetic field in the superconducting film. The domain pattern in the garnet was monitored optically and this enabled one to map the field immediately above the surface of the superconductor. In particular the response of the superconductor to an applied magnetic field was studied.

In general flux was observed to penetrate along the edges of a square sample with the penetration being far greater at the mid points of the edges than at the corners. As the field was increased the flux penetration eventually reached the centre of the film but the penetration along the diagonals was very weak. Maxwell's equations were used to analyze the data and hence obtain the current distribution in the films. Preliminary investigations of some superconducting device structures were also carried out but a lack of spatial resolution prevented a detailed study of actual junctions.

The magneto-optical technique described in this thesis is relatively inexpensive to assemble and yet provides a fast, effective means of monitoring flux penetration into a superconducting film. Given that the flux penetration is also observed to be very sensitive to the presence of defects, it is clear that the technique could find an application in quality control for thin film growers. Finally, it may be possible to carry out real time measurements of flux leakage and, given a garnet with small enough domain structure, one might be able to probe the vortex dynamics in high-T_c films.

Acknowledgments

This has been a collaborative project and I would like to thank several of my co-workers. I would like to express my gratitude to Dr. Bret Heinrich for many fruitful discussions that revealed aspects of superconductivity and magnetism directly related to this work. I would also like to express my thanks to Dr. Heinrich for his support during my attendance at a conference on the statics and dynamics of vortices in Eugene, Oregon. I am indebted to Dr. Sergei Govorkov for the experimental guidance he provided during the latter stages of the project. His experimental expertise proved to be invaluable in designing and constructing various components used in this experiment. I feel I have gained considerable knowledge from him and have benefited from his involvement in this project. The Hall probe data provided by Weibing Xing was used as a comparison to confirm our results. I would also like to thank Dr. Ilya Entin for providing the magnetization calculations that are presented in this thesis. Finally, I would like to thank my supervisor Dr. Chuck Irwin, for his support and guidance throughout this project.

The garnet film used to produce the images presented in this thesis was kindly donated by Vincent Fratello of AT&T Bell Laboratories and several of the superconducting films studied in this work were provided by CTF Systems Inc. The project described in this thesis was part of a larger collaborative effort called the High T_c Alliance Project. All members of the alliance have made contributions and I am particularly grateful for the financial support provided by CTF Systems, the Natural Sciences and Engineering Council of Canada, the Industry Canada (STP-AIM) program, the BC Ministry of Employment and Investment, Furukawa Electric Co., and Yokohama R&D Labs.

Table of Contents

List of Figures

Chapter 1
Introduction

The phenomenon of superconductivity was discovered in 1911 by Kamerlingh Onnes[1], who developed a technique to liquefy helium which in turn enabled him to examine the electrical resistance of metals at previously unattainable temperatures. He found that as mercury was cooled its resistance gradually decreased until a temperature of 4K whereupon it suddenly dropped to zero. Shortly thereafter a large number of elements and alloys where found to exhibit similar transitions at very low temperatures. The belief that this new state could be described simply by applying Maxwell's equations to a perfect conductor persisted for 22 years until work by Meissner and Ochsenfeld proved that this new superconducting state could not be described by conventional laws[1]. They observed complete magnetic flux exclusion from the inside of a sample, superconductors spontaneously became perfect diamagnets at the transition temperature.

To further complicate matters it was discovered that some features associated with superconductivity were not always obeyed. Some metals, especially alloys, did not exhibit a reversible magnetization but showed a strong hysteresis. It was also noted that in some cases the resistance and magnetic induction did not always go to zero at the same applied field. Thermodynamic arguments also predicted a specific heat discontinuity which was not observed in all samples. These results strongly suggested that there existed another superconducting state.

A theory presented by Ginzburg and Landau predicted that there were two types of superconductors. Type I superconductors show the perfect diamagnetic behavior associated with earlier experiments while type II superconductors allow a lattice of normal cores characterized by a region of magnetic flux to penetrate. Although type II superconductors allow the inclusion of normal regions they remain resistance-less at

much higher fields because there remains a superconducting current path through the sample.

Flux bundles that enter a superconductor may be moved by applying a current and this in turn develops a potential across the sample. In device applications it is desirable to use as much current as possible without dissipating energy. This is accomplished by preventing flux motion by incorporating various types of defects into the superconductor.

In general, type II superconductors have been utilized in technical applications due to their higher critical fields and critical currents. By examining the method by which flux bundles enter superconducting samples it is possible to determine properties that influence their effectiveness in applications. A measurement of the magnetic profile above the surface of the superconductor may give information on the screening currents and thus an estimate of the critical current. The spatial distribution of flux may also be used to determine effects of twin boundaries and crystal defects.

Thin films possess different characteristics from bulk samples, most notably a larger critical current which makes their study relevant to industry. High T_c thin films have found applications in micro-electronics. They have been used to make such devices as DC SQUIDs, microwave switches, filters, delay lines, and transmission lines.

Several techniques have been used to spatially resolve flux penetration in superconducting films. These include decorating the sample with fine magnetic particles[2], scanning Hall microscopy[3], scanning force microscopy[4], using a magneto-optically active glass[5] evaporating a thin magneto-optical layer of EuS on the sample surface[6] and using a magneto-optical garnet film[7]. These methods of flux visualization all have features which hinder their effective use as a flux probe technique. For example, the scanning Hall probe typically has a very large sensing area, thus limiting its resolution. This technique is also limited by the distance above the sample it may scan. The scanning force microscopy technique has excellent resolution but scans a very small area, limiting its ability to observe macroscopic phenomena. Magneto-optical methods

may yield near optical resolution and also probe a large surface area if needed, but they are somewhat limited in their field resolution by the Faraday rotation (deg/cm) constant of the material involved.

Weiss *et. al.* [2] have used a magnetic particle decoration technique to observe fluxoid lattices in single crystal YBCO samples. They examined the flux patterns as a function of applied field and determine preferential pinning sites along the **a,b,** and **<110>** directions. They also present some analysis on the long range order of the fluxoid lattice. The lattice parameter of their 8 G data appears to be approximately 2-3 μm. The technique involves evaporating fine iron particles in an inert gas such as helium and allowing these particles to decorate the superconducting sample. The pattern is then observed by scanning electron microscopy.

Presently garnet films and EuS layers are widely used as components in magneto-optical flux studies. EuS films have a better resolution than garnet films as garnets possess a domain structure that limits the resolution to the domain size. EuS also orders ferromagnetically but the optical effects of a large domain structure can be removed by adding EuF_2 [8]. This mixture eliminates large scale domains in favour of microscopic ones and thus allows these films to achieve optical resolution. The main disadvantage of EuS is its low Curie temperature (T_C=16.3) which limits its operation to liquid helium temperatures.

The advantages of garnet films include ease and rapidity of measurements, speed of image acquisition, operation in a wide temperature range, and its non-intrusive nature. The garnet may be used at any temperature below its Curie temperature (T_C=553K) which makes these films well suited for examining the magnetic characteristics of high Tc thin films. A simple optical cryostat operating at liquid nitrogen temperature was used in the present study.

This thesis describes a magneto-optical imaging technique based on garnet films, that can be used to measure weak magnetic fields near the surface of a superconducting

film. The present investigation uses a uniaxial anisotropic garnet film to obtain high resolution images of the magnetic field penetration using the Faraday effect. In particular the film used in this experiment was an yttrium iron garnet. This film had a domain width of approximately 6 μm and completely saturated in an applied field of 30 Oe. This limits the magnetic field range and spatial resolution at the present time.

By placing this film on top of a superconductor, the magnetic field due to superconducting shielding currents may be visualized. The garnet film consists of domains having a highly perpendicular uniaxial anisotropy which results in a magnetization perpendicular to the surface. The magnetization changes alternately between up and down as one crosses domain boundaries. Each of these domains (up and down) rotates polarized light by a specific angle ($\pm\theta$), allowing the magnetic structure of the garnet to be seen via the Faraday effect. Polarized light is passed through the film and examined using an analyzer (another polarizer). The analyzer is rotated until an optimum contrast (dark and light) is obtained between up and down domains. When an external field is applied, the domain walls move enlarging domains parallel to the field and shrinking those anti-parallel. The resulting light intensity may be averaged over a region of the film greater than the width of the individual domains. This intensity is proportional to the applied field.

The remainder of this thesis describes measurements of the flux penetration in thin films of $YBa_2Cu_3O_{7-x}$ and $Tl_2Ba_2CaCu_2O_8$. The regions along film diagonals have been found to effectively shield external fields. Flux was also found to penetrate in small rivers from defects along edges. A current distribution was obtained by calculating the magnetization of the sample using measured field data.

A scanning Hall probe confirmed the results obtained. This probe was significantly further away from the surface and had a much coarser resolution than the garnet film, nevertheless, the scans corresponded very well with the garnet images.

The magneto-optical technique is not new, as Huebener[9] used EuS in 1970 to image Nb films. Recently several experiments have been carried out on $YBa_2Cu_3O_{7-x}$ films with similar results. Twin boundaries have been found to act as penetration vents by Duran[10], Turchinskaya[11], and Vlasko-Vlasov[12] using a magneto-optical technique.

The properties of the magneto-optical garnet films will be reviewed in more detail in Chapter 2. in relation to the present experiment. Chapter 3 provides a brief overview of the phenomenon of superconductivity and Chapter 4 outlines the experimental setup and procedure used to map the magnetic flux above the surface of a superconducting sample. Chapter 5 presents some of the results obtained and finally chapter 6 presents conclusions and suggestions for further work.

Chapter 2
Garnet Films

2.1 Physical Properties of Garnet Films

Garnet films are ferromagnets possessing a complicated domain structure. The domain walls move under the influence of an applied magnetic field allowing a the local magnetic field strength to be determined by averaging the magnetization over several domains. Under certain conditions (determined by the manufacturing process) these films form circular domains called magnetic bubbles. In the past magnetic bubbles have been used as memory devices. The film used in the present study consisted of strip domains which orient themselves in such a way so as to minimize the total energy (magneto-static energy, domain wall energy, and the applied field energy) of the film.

The basic chemical formula for a magnetic iron garnet is $R_3Fe_5O_{12}$ where the R is a rare earth or yttrium. Garnets are cubic with a strong crystalline anisotropy along the body diagonals. A uniaxial magnetic anisotropy may be induced by a lattice mismatch with the substrate, or may be growth induced. A growth induced anisotropy results from impurity atoms which are present as the film is made, examples are lead and bismuth which are contained in the flux that is used as a solvent. These ions occupy yttrium sites.

The unit cell of a yttrium iron garnet contains 160 atoms including 96 O ions, 24 Fe ions occupying tetrahedral sites(d), 16 Fe ions occupying octahedral sites(a), and 24 Y ions occupying dodecahedral (c) sites. Figure 2.1 shows a section of the unit cell indicating which sites are occupied by yttrium, iron and oxygen atoms. The actual unit cell is cubic and made up of a complicated arrangement of (a), (d) and (c) sites.

The magnetic moments of ions in the (a) and (c) sites are parallel while the remaining moments corresponding to ions in (d) sites are anti-parallel. In a rare-earth garnet (i.e. Y replaced by a rare-earth) the moment of the (c) sites is strongly temperature dependent and leads to a magnetization shown in figure 2.2. Because of this effect, there

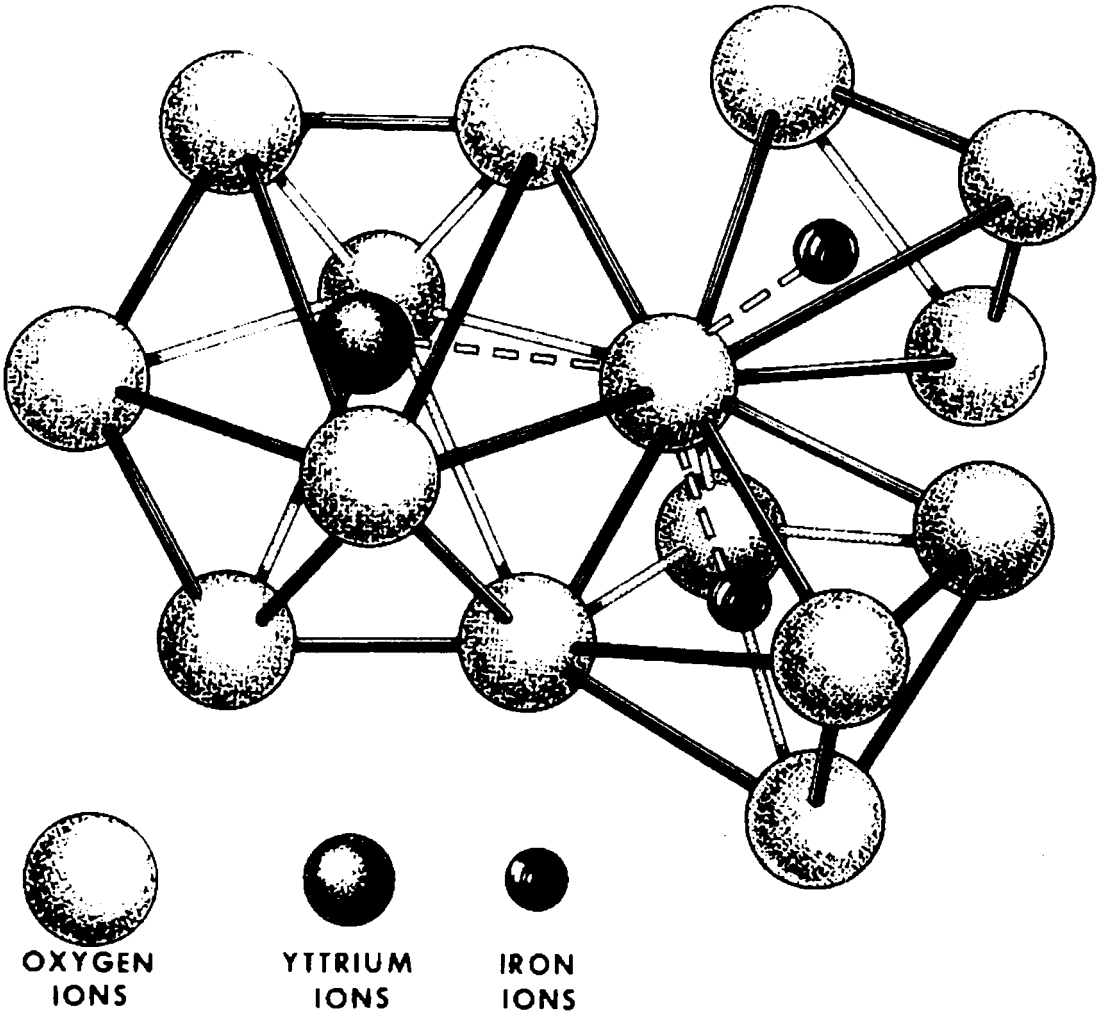

Figure 2.1 Section of yttrium iron garnet unit cell (used with permission Bobeck and Torre[13]). The yttrium atom on the left surrounded by eight oxygen atoms forms a dodecahedral (c) site. The iron atom on the upper right surrounded by four oxygen atoms forms a tetrahedral (d) site. The iron atom on the lower right surrounded by six oxygen atoms forms a octahedral (a) site. The unit cell is formed by an arrangement of similar units with different orientations.

is a temperature at which the moments due to the (a) and (c) sites exactly cancel the moment of the (d) site, leading to a magnetization of zero. This temperature is known as the compensation temperature.

The moment of each sub-lattice for a gadolinium iron garnet is shown in figure 2.3. In the present experiment an yttrium iron garnet was used. The yttrium sublattice has no moment of its own, implying the saturation magnetization will be dominated by the iron atoms in the (d) sites. This may be observed in figure 2.3, the moment associated with the dodecahedral sites M_C will be zero and $|M_d| > |M_a|$.

The magnetization of the film may be changed by replacing iron with gallium ions, which will occupy the (d) sites thus reducing the effective moment since gallium is non-magnetic. When the gallium ion count is 1.34 per formula unit the garnet becomes non-magnetic[14]. The composition of the magnetic iron garnet used in this experiment is $Bi_{0.29}Pb_{0.04}Y_{2.67}Fe_{3.9}Ga_{1.1}O_{12}$.

Bismuth substitution is an important factor governing the operating characteristics of yttrium iron garnets. It increases the anisotropic energy of the film and reduces the coercive force (the minimum force needed to move a domain wall). Matsumoto *et. al.* [15] have examined the large Faraday rotation associated with heavy bismuth doping (<2 atoms per formula unit) and have found theoretical expressions for the Faraday rotation as a function of bismuth content.

The magnetic yttrium iron garnet film is grown on the top of a non-magnetic gadolinium gallium garnet (GGG). The chemical composition of the GGG substrate is $Gd_3Ga_5O_{12}$. The substrate is chosen so that the lattice parameter of the substrate and the film match well enough for good epitaxial growth. If the garnet film is to be used for high resolution magnetic field measurements, the substrate must also be non-magnetic and relatively free of defects. Typically GGG substrates may be grown with a surface roughness of $\approx 3\mu m$ [16], and dislocation densities of $0.5/cm^2$.

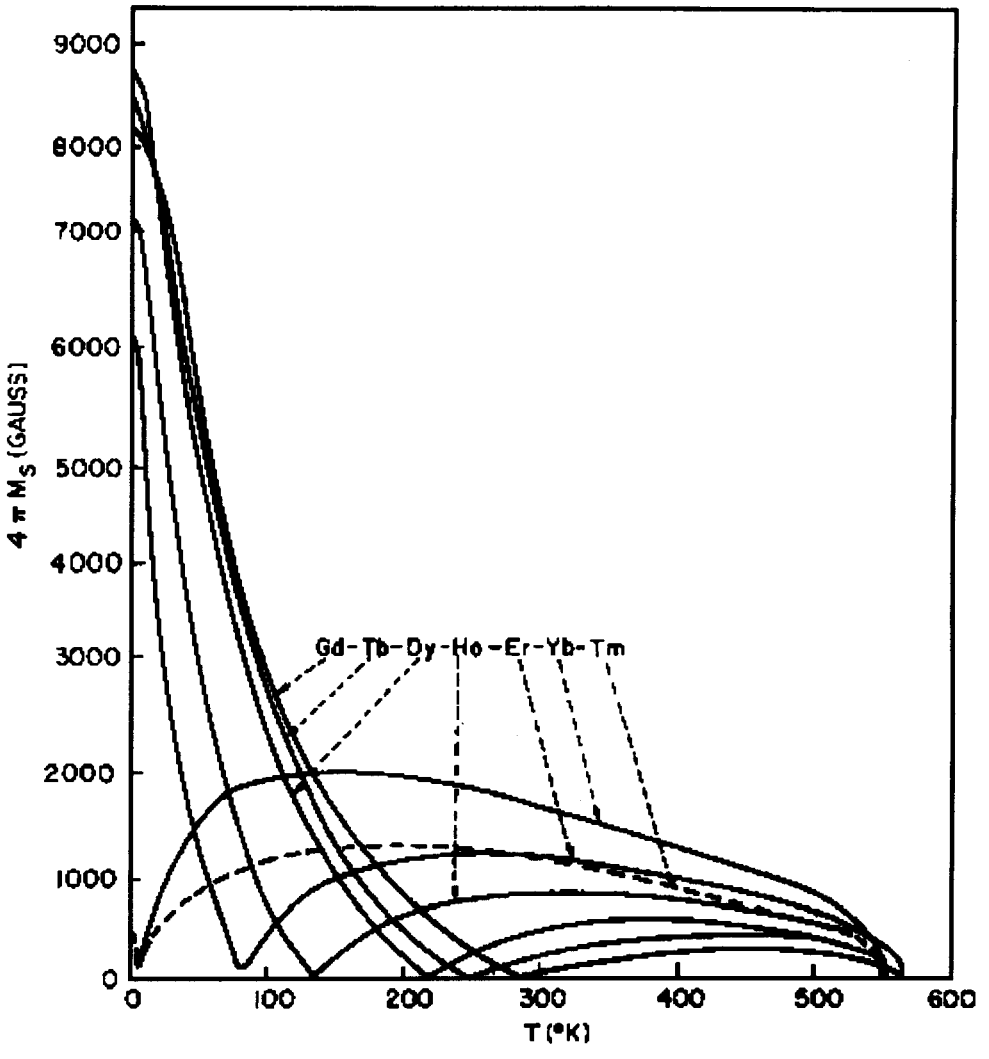

Figure 2.2 Magnetization of various types of garnets (used with permission, Bobeck and Torre[13]).

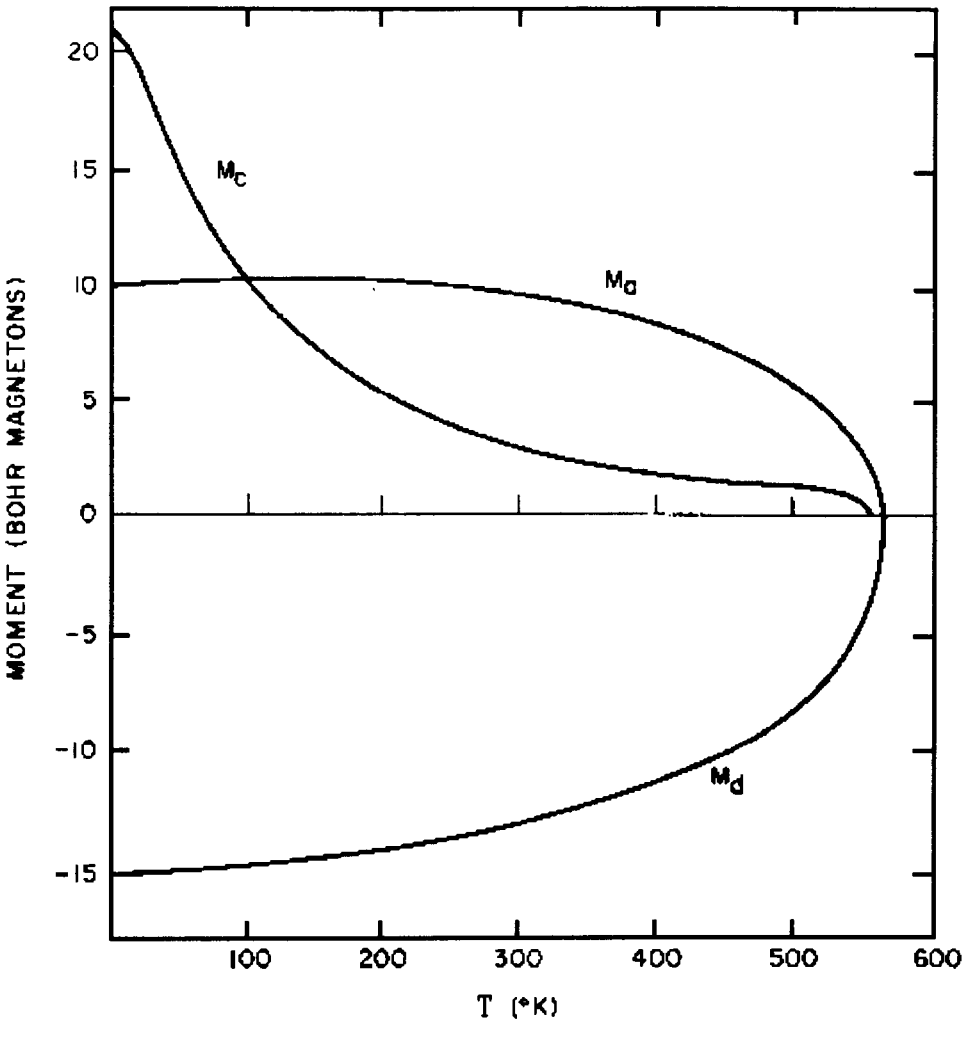

Figure 2.3 Magnetization of different sublattices of Gadolinium Iron Garnet (used with permission, Bobeck and Torre[13]). M_a and M_d represent the magnetization due to the octahedral and tetrahedral iron sites. M_c is the magnetization due to the dodecahedral Gadolinium sites.

2.2 Parameters Characterizing Garnet Films

Garnet films have been used previously in computer memory devices and are now being applied to fiber optic technology[17]. A number of physical parameters determine the operating characteristics of garnet films, and these are important in determining the usefulness of the particular film in device applications. The following section gives a brief overview of some of these parameters and their importance.

2.2.1 The Anisotropy Energy

Ferromagnetic materials exhibit a preferential direction (easy axis) along which the field required to induce a magnetization is a minimum. In other words, along certain crystallographic directions a smaller field is needed to completely magnetize the material. Thus there is an anisotropy in the magnetic energy of the crystal. It is defined as the excess energy required to magnetize a crystal in a given direction over that required for an easy axis magnetization[18].

In the case of a garnet film with its easy axis perpendicular to the surface the anisotropy energy density may be expressed as

$$E_k = K_u \sin^2 \phi \qquad (1)$$

where ϕ is the angle of the magnetization with respect to the easy axis, and K_U depends on the film and is known as the uniaxial anisotropy parameter.

There exist two types of anisotropy, namely the crystalline anisotropy inherent to the material and the induced anisotropy produced during the growth process. A uniaxial magnetic anisotropy may be induced in the crystal by stress, provided by a mis-match in the film-substrate lattice parameters, or growth methods in which impurities are added to produce an easy axis of magnetization perpendicular to the surface of the film. The garnets possess a cubic lattice. The growth induced anisotropy dominates over a weak crystalline anisotropy.

In the case of a thin film there is an extra demagnetization energy density of $2\pi M_s^2$ for a magnetization perpendicular to the film[19] (with respect to the energy density of a configuration with a magnetization in the plane of the film). The anisotropic energy density must be larger than the demagnetization energy density to maintain a magnetization perpendicular to the film's surface. Therefore, unless the quality factor

$$Q = \frac{K_u}{2\pi M_s^2} > 1 \qquad (2)$$

the ferromagnetic material will have a magnetization in the plane of the film.

2.2.2 The Exchange Energy

A ferromagnetic material has the magnetic moments of neighbouring atoms aligned parallel to each other at sufficiently low temperatures. The magnetic moments remain in this state until the Curie temperature T_C, where thermal agitation breaks the coupling between neighbors and the material becomes para-magnetic. Two parallel magnetic moments possess an exchange energy of $-E_{ex}$, whereas anti-parallel moments have an energy of $+E_{ex}$. For $k_bT < |E_{ex}|$, a ferromagnetic material has parallel moments and possesses magnetic properties. The exchange energy E_{ex} is approximately k_bT_C where T_C is the Curie temperature. A ferrimagnetic material such as the YIG used in this experiment, possesses several sub-lattices with alternating parallel and anti-parallel moments. In an yttrium iron garnet the (a) and (d) sites possess a positive exchange interaction with members of the same sublattice. The exchange interaction is negative however, between members of the (a) and (d) sublattices.

2.2.3 The Domain Wall Energy Density

Domain boundaries are regions where the magnetic moment makes a smooth transition from one direction to the other. Each individual moment will be at a small angle with its neighbor such that the total angle traversed through the domain wall is 180 degrees. The exchange energy is not at its minimum value of $-E_{ex}$ inside a domain wall

but at a slightly higher value of $-E_{ex}\cos\phi \approx -E_{ex}(1-\phi^2)$ where ϕ is the angle between neighboring moments. The total increase in energy as the wall is traversed is given by

$$\Delta E_{ex} \approx NkT_c\phi^2\delta/2 \tag{3}$$

where N is the density of atomic moments and δ is the width of the domain wall. If the moments are separated by a distance a ($N=1/a^3$), then the angle ϕ is given by $\frac{\pi a}{\delta}$, and

$$\Delta E_{ex} \approx NkT_c\pi^2a^2/2\delta \tag{4}$$

The domain wall energy is minimized for a very wide wall.

The anisotropic energy favours a narrow wall. The width of a domain wall will be determined by competition between the exchange energy and the anisotropic energy. The anisotropic energy density is given by $K_u\sin^2\psi$ where ψ is the angle between the magnetic moment and the easy axis. The increase in wall energy is given by

$$\Delta E_k = K_u\int_0^{\delta}\sin^2\frac{\pi x}{\delta}dx = \frac{K_u\delta}{2} \tag{5}$$

Combining equations (4) and (5) the total wall energy density is

$$\sigma_w = \frac{kT_c\pi^2}{2a\delta} + \frac{K_u\delta}{2} \tag{6}$$

2.3 Domain Wall Dynamics

When the magnetization is oriented perpendicular to the film it has an extra demagnetization energy of $2\pi M_s^2$ This energy is minimized when strips of alternating magnetization are formed. The demagnetization energy is minimized when the volumes of the domain structures are equal giving a macroscopic magnetization of zero. A serpentine like structure can be formed as shown in figure 2.4.

Under the influence of an applied field, the domain walls move such that one domain is enlarged at the expense of its neighbors. As a rough approximation to the

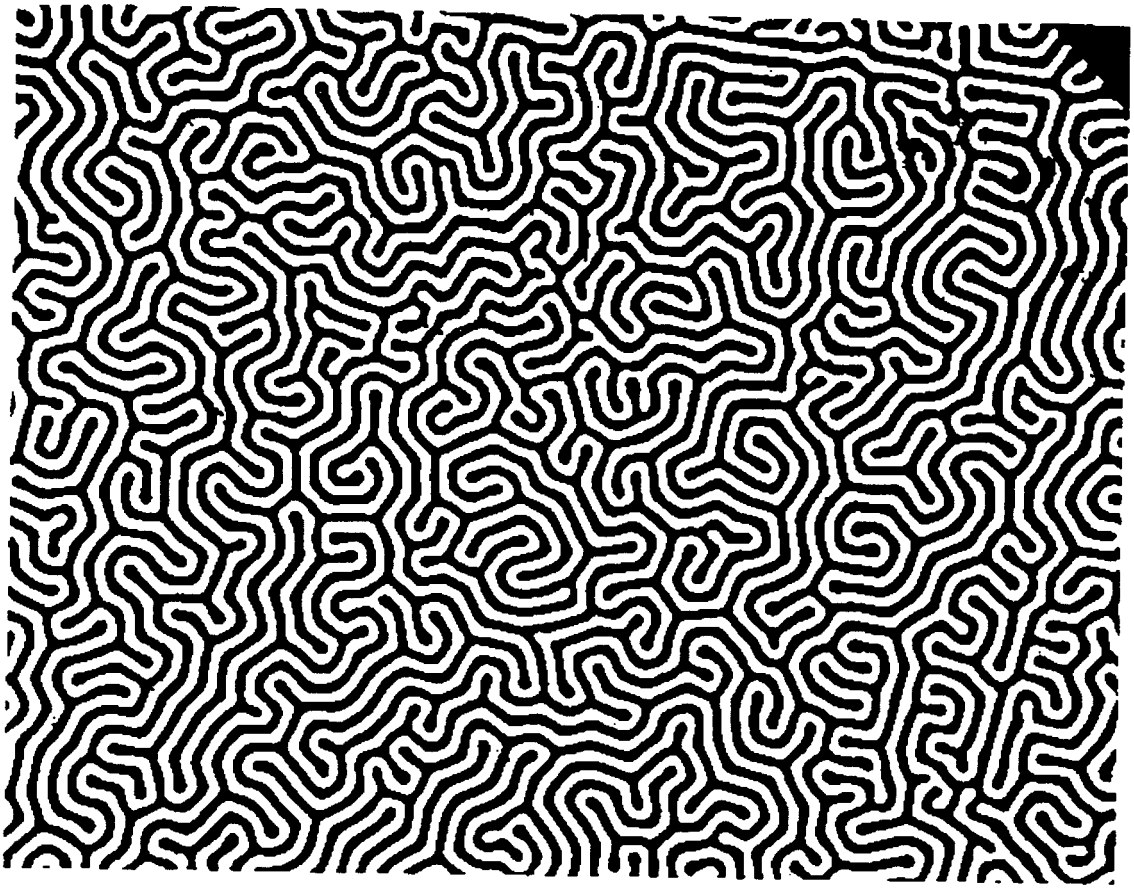

Figure 2.4 Domain structure of a garnet film at room temperature.

observed strip structure, Bobeck [13] developed a model to determine the width of a series of parallel strip domains as a function of the applied field. The total energy density of the system consists of contributions from three different terms, the domain wall energy W_w, the applied field energy W_h, and the internal magneto-static energy W_m,

$$W=W_w+W_h+W_m \tag{7}$$

If two domains with a total width d ($d=d_+ + d_-$ where d_+, d_- are the widths of each domain) are examined then the first term is

$$W_w = \frac{2h\sigma}{d} \tag{8}$$

where σ is the domain wall energy density of section 2.2.3 (equation 8). and h is the film thickness. The second term is

$$W_h=-\int_V \mathbf{M}\cdot\mathbf{H}_{applied}dV = -\frac{d_+ - d_-}{d} HM_s h \tag{9}$$

The internal magnetic energy is

$$W_m=-\frac{1}{2}\int_V \mathbf{M}\cdot\mathbf{H}_{int}dV \tag{10}$$

Using magnetic pole theory Bobeck[13] found the expression for the internal magneto-static energy W_m,

$$W_m=\frac{2M_s^2 d}{\pi^3}\sum_{n=1}^{\infty}\frac{1}{n^3}\sin^3\left[\frac{n\pi}{2}\left(1+\frac{M}{M_s}\right)\right]\left[1-\exp\left(-\frac{2n\pi h}{d}\right)\right] \tag{11}$$

The macroscopic magnetization M is given by $\frac{M}{M_s}=\frac{d_+ - d_-}{d}=2\frac{d_+}{d}-1$. To find a stable configuration of the system the following conditions must be applied to the total energy

$$\frac{\partial W}{\partial M}=0 \ , \ \frac{\partial W}{\partial d}=0 \tag{12}$$

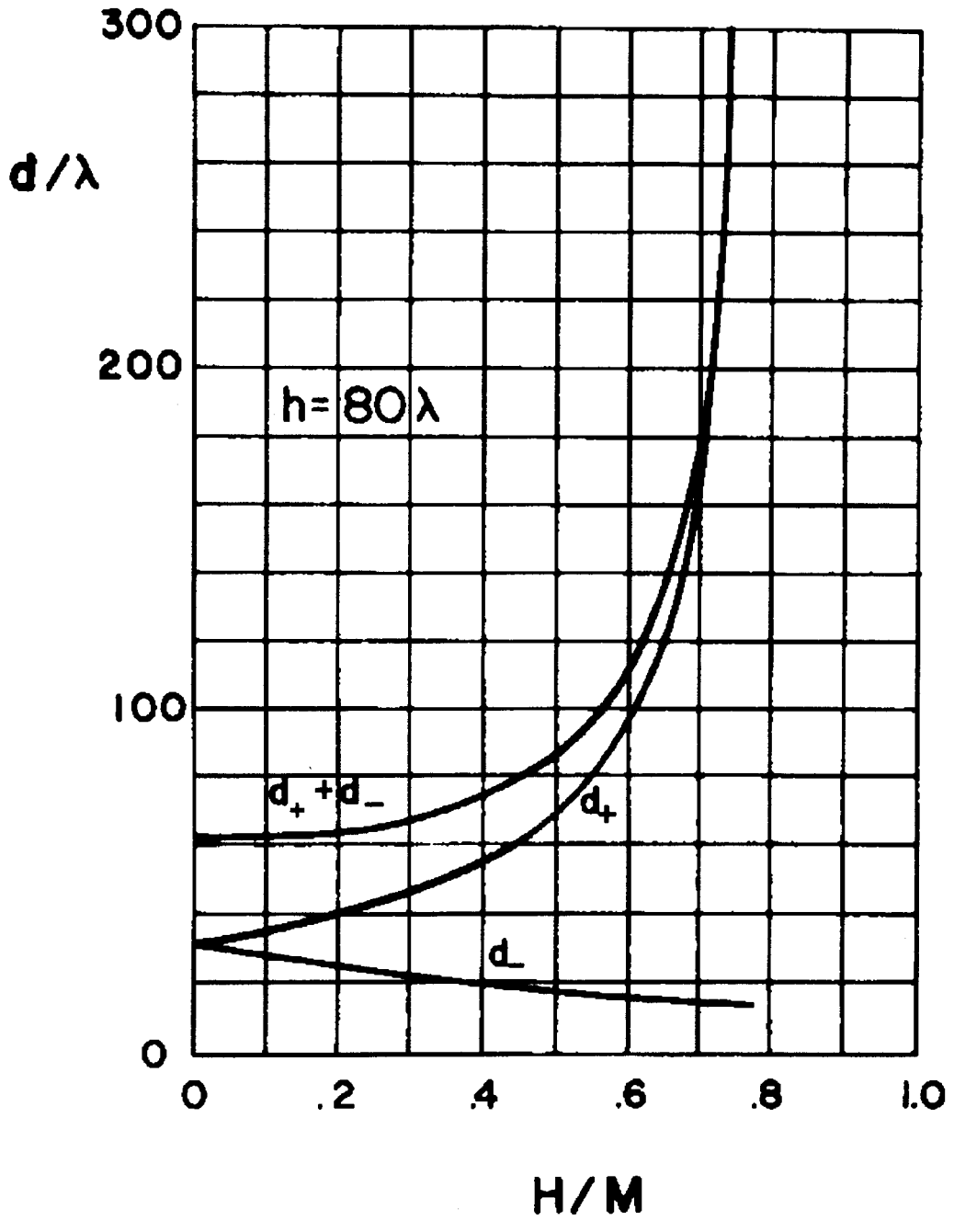

Figure 2.5 Domain widths as a function of applied field (used with permission, Bobeck and Torre[13]). The thickness of the film (h) and the domain widths (d_+ , d_-) are normalized to the characteristic length (λ) which is typically 1 μm. d_+ is the width of the domain magnetized in the direction of the applied field while d_- is the width of the other domain magnetized opposite to the applied field.

The resulting equations were solved simultaneously and plotted. The film thickness and strip widths are normalized to the characteristic length $\lambda = \frac{\sigma}{4\pi M_s^2}$ and the applied field is normalized to the magnetization M. At low fields, a linear response in the magnetization is evident in figure 2.5, however at high fields the strip is seen to collapse. The garnet film used in this experiment starts to collapse around 20 Oe.

2.4 The Magnetic Field Produced by a Garnet Film

The yttrium iron garnet film may be used to image magnetic flux (the technique will be described in greater detail in chapter 4). The garnet film is ferromagnetic and as such has a field of its own which may influence the superconducting sample being imaged. The following section gives an estimate to the magnitude of this field.

Each domain in the garnet film may be considered uniformly magnetized in one direction. The magnetic field will then be due to surface currents at the domain boundaries. The following is a derivation of the magnetic field of an infinitely long single strip domain. The result will then be applied to a series of adjacent strip domains giving an approximation to the magnetic fields associated with the garnet film. The thickness of the garnet film is t=1.3μm and the domains are 6μm wide. The saturation magnetization of the garnet is $4\pi M_S$=220 G.

Figure 2.6 shows microscopic currents in the garnet film which cancel in the interior of the domain while adding along boundaries. These effective domain wall currents flowing along domain boundaries produce a magnetic field above the surface of the garnet film. The magnitude of these currents is given by the magnetization.

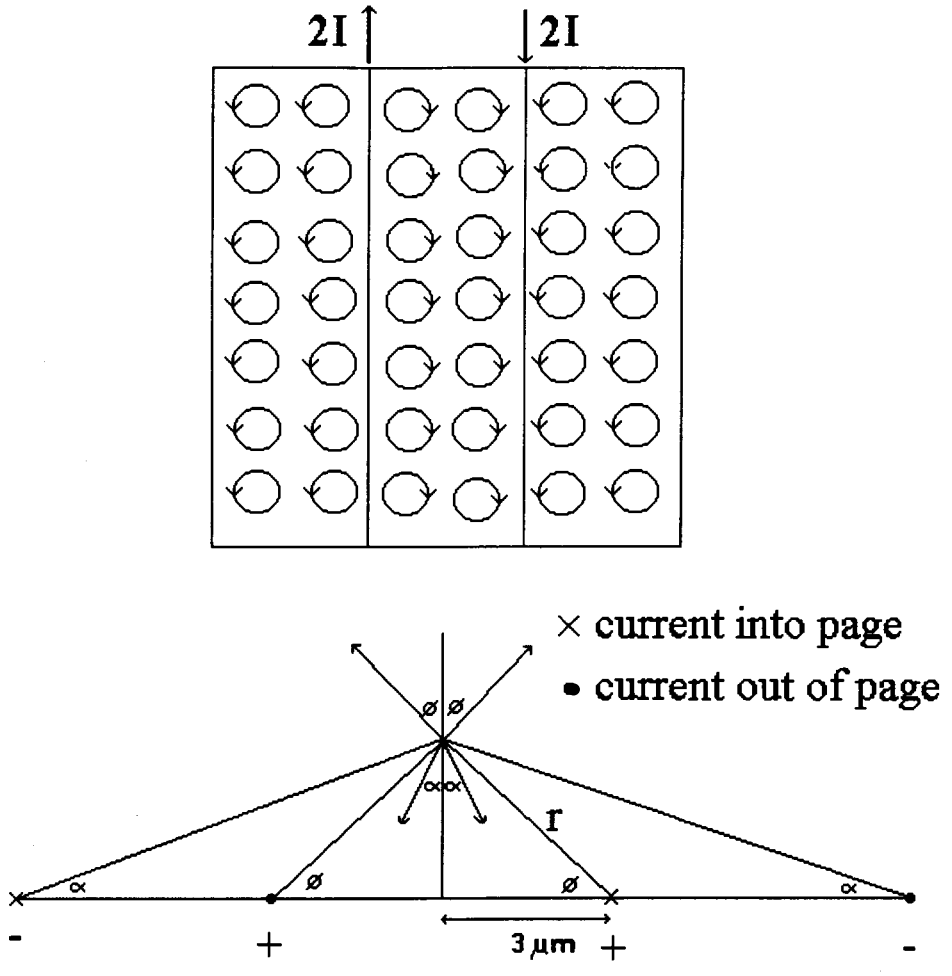

Figure 2.6 Contribution to the Magnetic field of a garnet film from its domains. The domain walls are marked with positive and negative signs to indicate which direction the walls contribute to the vertical magnetic field.

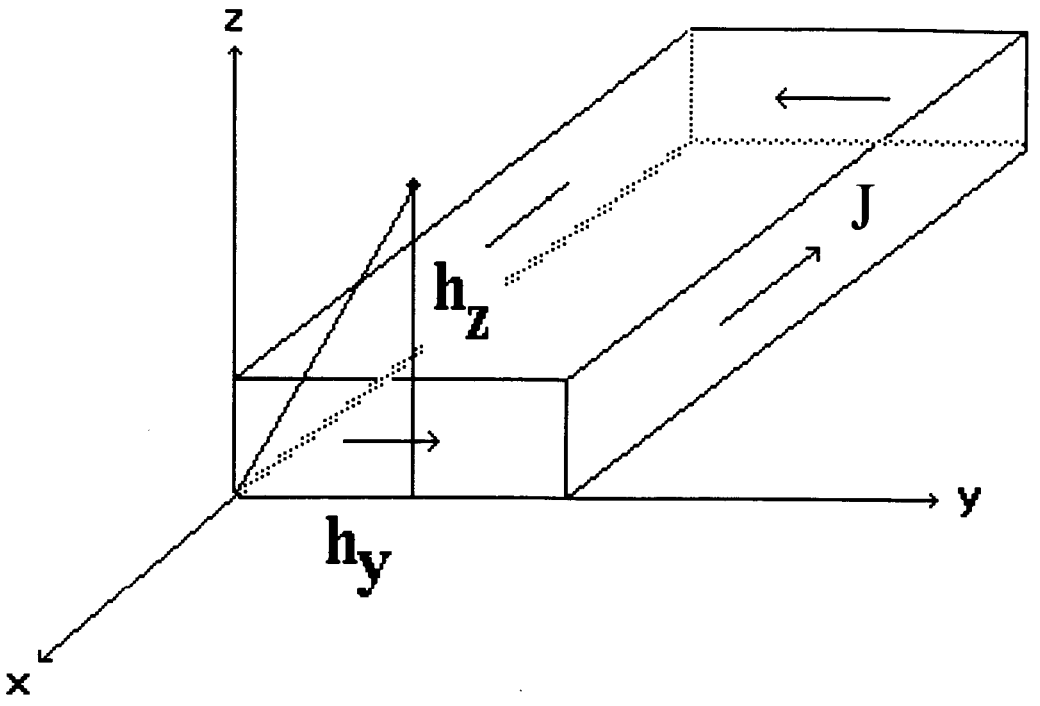

Figure 2.7 Surface current of a uniformly magnetized slab. The variables h_y and h_z refer to a point in space where the magnetic field is to be evaluated.

If one writes the vertical component of the magnetic field due to an arbitrary domain wall (as a function of variables shown in figures 2.6) one obtains

$$B_z = 4M_s \int \frac{\cos\phi}{r} dz \tag{13}$$

where the integration over z is down the domain wall. If one considers two adjacent domain walls the contribution to B_Z of each wall is opposite on either side but the same in the middle. Therefore we can introduce an index i where $(-1)^i$ will account for the sign of the field contribution for every wall in a sequence, this magnetic field contribution will change sign as one crosses the point h_y (as shown in figure 2.6 where +-+-+-+ → +-+-+-+). The variables ϕ and r may be written in terms of y and z. Including the index i, a domain width w (in the present case w=6 μm and the film is 1.3 μm thick), and referring to an origin located at the left edge of the film,

$$\cos\phi = \frac{w\cdot i - h_y}{\sqrt{(h_z - z)^2 + (w\cdot i - h_y)^2}} \qquad \frac{1}{r} = \frac{1}{\sqrt{(h_z - z)^2 + (w\cdot i - h_y)^2}} \tag{14}$$

If several strips are placed in a series the current flowing along a boundary will be doubled due to the addition of two surface currents at the domain wall. The contributions at i=0 and i=N will be half as large because there is only one domain at the edge. Combining expressions 13 and 14, one obtains for a series of N walls

$$B_z = 4M_s \sum_{i=1}^{N-1} (-1)^i \int_0^{1.3} \frac{w\cdot i - h_y}{(h_z - z)^2 + (w\cdot i - h_y)^2} dz \tag{15}$$

$$+2M_s \int_0^{1.3} \frac{w\cdot i - h_y}{(h_z - z)^2 + (w\cdot i - h_y)^2} dz + 2M_s (-1)^N \int_0^{1.3} \frac{w\cdot i - h_y}{(h_z - z)^2 + (w\cdot i - h_y)^2} dz$$

The sign change in the factor $(-1)^i$ as one passes by the point h_y is included in the equation as the integrand is an odd function with respect to h_y. Integrating the result becomes, (the first domain on the left is negative)

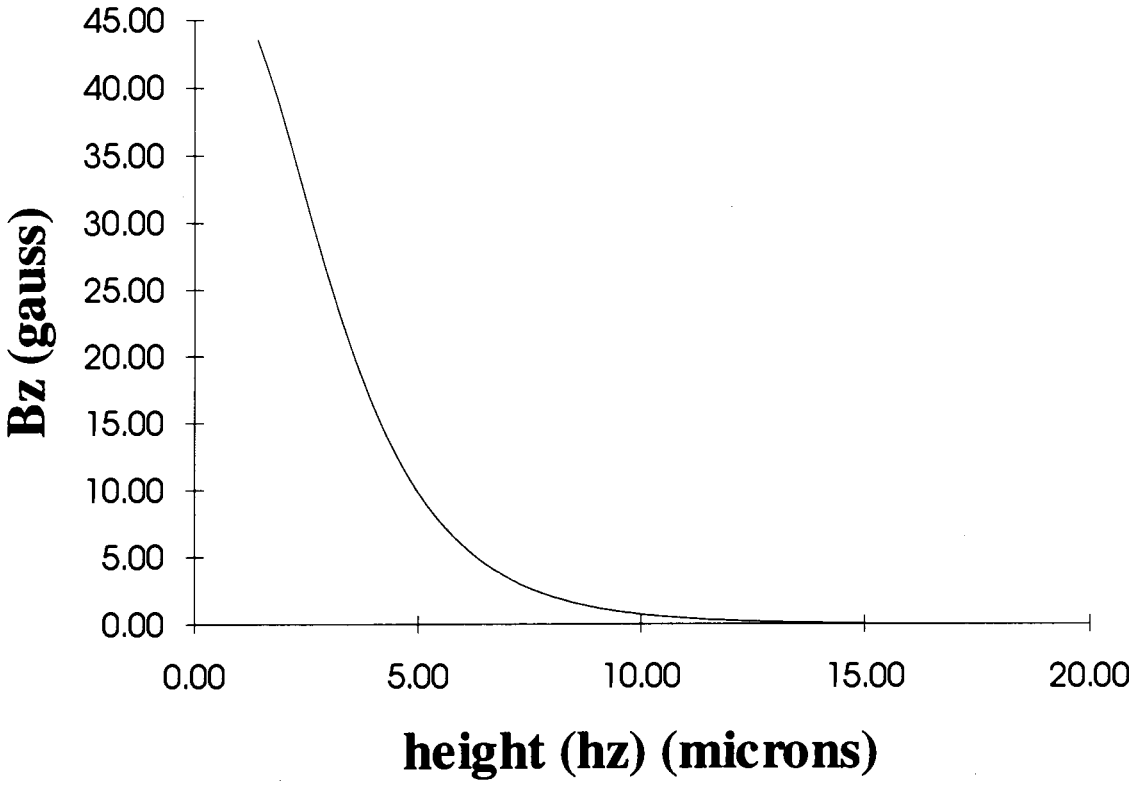

Figure 2.8 Vertical component of the magnetic field above the centre of a series of 50 uniformly magnetized strips. The strips are 6 μm wide and 1.3 μm thick. The field was calculated above centre of the middle strip. The height is referenced to the bottom of the film as shown in figure 2.7.

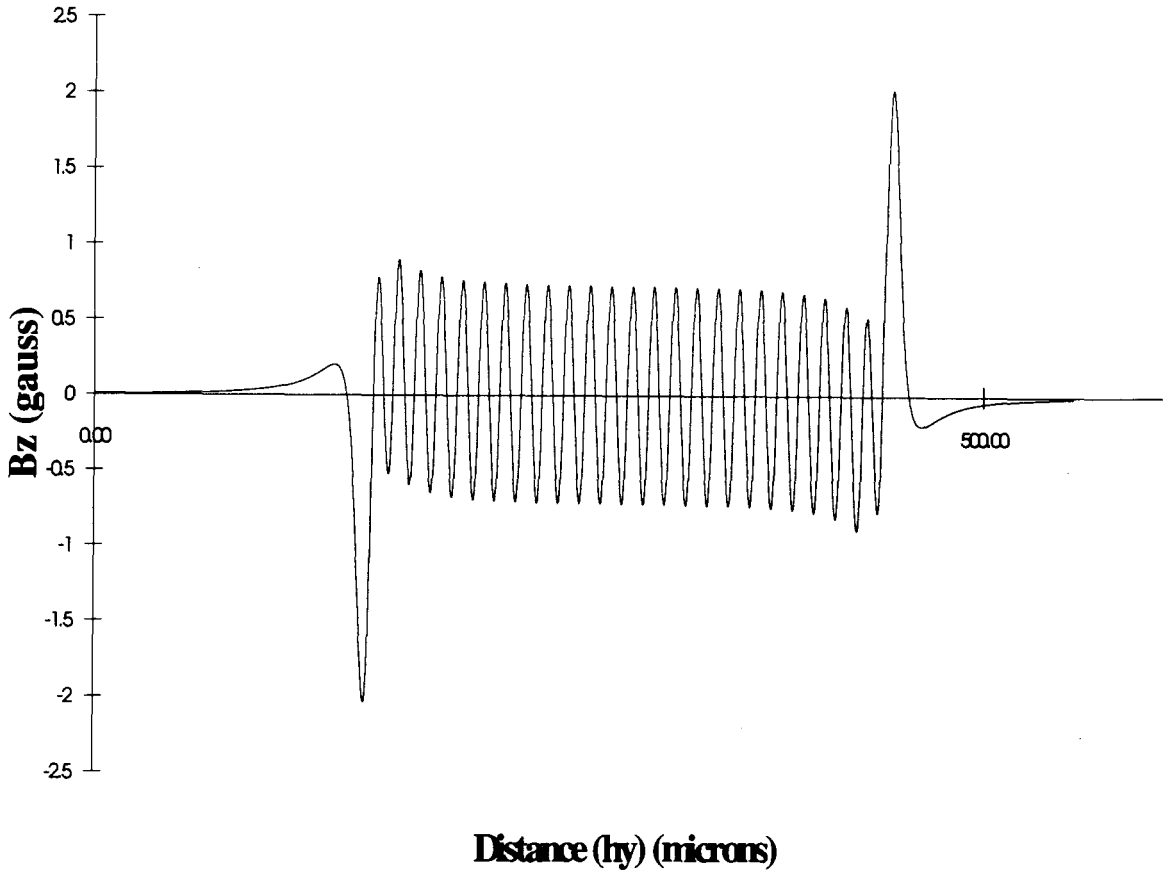

Figure 2.9 Vertical component of the magnetic field across 50 uniformly magnetized strips, 10 microns above the surface. The strips are 6 μm wide and 1.3 μm thick. The magnetized slabs lie between 150 and 450 microns.

$$B_z = 4M_s \sum_{i=1}^{N-1} (-1)^i \left[\tan^{-1} \frac{h_z - 1.3}{w \cdot i - h_y} - \tan^{-1} \frac{h_z}{w \cdot i - h_y} \right] \qquad (16)$$

$$+2M_s \left[\tan^{-1} \frac{h_z - 1.3}{w \cdot i - h_y} - \tan^{-1} \frac{h_z}{w \cdot i - h_y} \right] + 2M_s (-1)^N \left[\tan^{-1} \frac{h_z - 1.3}{w \cdot i - h_y} - \tan^{-1} \frac{h_z}{w \cdot i - h_y} \right]$$

The saturation magnetization of the garnet film used in this experiment is $4\pi M_s = 220G$ giving a prefactor of $2M_S$=35 for equation 15 (giving B_Z in units of Gauss). The vertical component of the field will have a maximum in the centre of a domain. The adjacent current lines contribute a positive component to this value (in a positive domain), the next two a negative component, the next two a positive component and so on. Using the field distribution for an infinitely long strip domain calculated above, and applying the result to a series of fifty strips, one obtains the field strength above the film as a function of distance, as shown in figure 2.8.

The above result may also be used to calculate the field distribution across the sample. Figure 2.9 shows the field profile 10 μm above a series of 50 uniformly magnetized strips.

In conclusion, it is not likely the garnet will have a great effect on the superconductor it is trying to image. The distance between the superconducting film and the garnet film is determined by the surface roughness of each, and is estimated to be on the order of 10 μm. This gives a contribution of a fraction of a gauss according to figure 2.8. The actual magnetic field is even smaller than the calculated field, due to the random distribution of domains as shown in figure 2.4.

Chapter 3

Superconductivity

3.1 London Theory of Superconductivity

The absence of electrical resistance at sufficiently low temperatures was first thought to be the result of superconducting electrons which coexisted with their normal counterparts. A thermodynamic treatment of such a two fluid model was first done by Gorter and Casimir in 1934 [1]. This model predicts the fraction of superconducting electrons to be 100% at absolute zero and gradually decreases to zero at the transition temperature T_C. The two fluid model was successful in describing various thermal properties of superconductors found through experiment. When combined with London's electro-magnetic theory the two fluid model correctly predicts the temperature dependence of the magnetic penetration depth λ_L [20] (the depth at which a magnetic field drops to 1/e of its value outside the superconductor).

If one assumes a particle with an effective charge e and an effective mass m obeys $\frac{dv}{dt} = \frac{e}{m}E$, then from $J = n_s ev$ (n_S is the superconducting electron density), one obtains

$$\mathbf{E} = \frac{m}{n_s e^2}\frac{d\mathbf{J}}{dt} \tag{1}$$

Combining this with the Maxwell equation,

$$\nabla \times \mathbf{E} = -\frac{1}{c}\frac{d\mathbf{H}}{dt} \tag{2}$$

one obtains,

$$\frac{n_s e^2}{mc}\frac{d\mathbf{H}}{dt} + \nabla \times \frac{d\mathbf{J}}{dt} = 0 \tag{3}$$

London found he could account for the perfect diamagnetic behavior of superconductors by integrating equation 3 and taking a particular solution

$$\frac{n_s e^2}{mc}\mathbf{H} + \nabla \times \mathbf{J} = 0 \tag{4}$$

On inserting Maxwell's equations

$$\nabla \times \mathbf{H} = \frac{4\pi}{c}\mathbf{J} \quad \text{and} \quad \nabla \cdot \mathbf{H} = 0 \tag{5}$$

one obtains

$$\nabla^2 \mathbf{H} + \frac{4\pi n_s e^2}{mc^2}\mathbf{H} = 0 \tag{6}$$

The perfect diamagnetic behavior of superconductors is predicted by equation (6). For a superconducting material filling the volume x<0 in the presence of a field H_0 applied parallel to the surface this equation has the solution

$$H = H_0 \exp(-x/\lambda_L) \tag{7}$$

According to this equation the field drops exponentially from the surface with a characteristic length defined by $\lambda_L = \sqrt{\frac{mc^2}{4\pi n_s e^2}}$ which is known as the London penetration depth[21]. Application of the remaining Maxwell's equations shows that the surface currents flow at the edge of the sample (within the penetration depth λ_L), creating a field in the interior which cancels the applied field.

The London theory succeeds in predicting the diamagnetic behavior of superconductors at low fields but fails in the high field limit. A more complete theory was given by Ginzburg and Landau in 1950.

3.2 Ginzburg-Landau Theory

The theory developed by Ginzburg and Landau[22] describes the superconducting state in terms of an order parameter ψ and the free energy of the superconducting system. The order parameter is a complex wavefunction representing the density of superconducting charge carriers. The free energy may be described by the Gibbs thermodynamic potential

$$G = U + PV + TS \tag{8}$$

where U is the internal energy of the system and P,V,T,S are pressure, volume, temperature, and entropy respectively. Applying various thermodynamic relations and including a term due to the magnetic energy of the system one finds

$$dG = VdP - SdT - VM \cdot dH \tag{9}$$

The Gibbs potential is constant during a second order phase transition, which implies

$$G_n = G_s(H_c) \tag{10}$$

where G_n is the Gibbs energy in the normal state, G_S is the Gibbs energy of the superconducting state and H_C is the critical field at which the superconducting-normal transition takes place. In the case of a perfectly diamagnetic superconductor in the presence of a field H_a, the Gibbs free energy per unit volume is

$$G_s(H) = G_s(0) + \frac{H_a^{\,2}}{8\pi} \tag{11}$$

at constant temperature and pressure. This expression is valid in the absence of a demagnetization field and under the assumption that the magnetization of a superconductor is simply $M = -\frac{H}{4\pi}$.

Ginzburg and Landau then introduced an extra term to the free energy to represent the change in energy due to the spatial variation in superconducting properties. The resulting equation is

$$G_s(H) = G_s(0) + \frac{H^2}{8\pi} + \frac{1}{2m}\left[-i\hbar\nabla\Psi - \frac{e^*}{c}A\Psi\right]^2 \tag{12}$$

where A is a magnetic vector potential and e^* is an effective charge. The free energy density may be expressed in terms of the order parameter in the limit T→Tc, $G_s = G_n + \alpha|\Psi|^2 + \beta|\Psi|^4 + \ldots$. This equation is solved by minimizing the volume integral of the free energy density with respect to the vector potential A and the order parameter ψ. The two equations are solved simultaneously and yield expressions for the spatial variation of ψ as well an expression relating the current density to the vector potential. In

the low field limit, the Ginzburg-Landau equation yields a result similar to the London theory. This theory was also successful in predicting the existence of a new class of superconducting materials in which the zero resistance state be could maintained above Hc.

3.3 Microscopic BCS Theory

The Ginzberg-Landau theory provided a method of describing the electro-magnetic properties of superconductors in high fields. It did not explain the observed discrepancies that were found in the critical temperature when different isotopes of the same material were examined. This phenomenon indicated that superconductivity was somehow related to an interaction between electrons and the crystal lattice. A non-local microscopic theory was developed by Bardeen, Cooper and Schrieffer[23] (BCS) in 1957 to describe the phenomenon of superconductivity based upon quantum mechanical arguments. They found that a phonon-electron interaction could be used to account for the absence of electrical resistivity in a superconductive state. The free energy of the superconducting state would be lowered relative to the normal state if two electrons could form a bound pair mediated by an attractive potential between them. There exists a weak attractive potential that arises between two electrons in a vibrating crystal due to ionic motion. This potential is too weak to form a bound electron pair by itself, but Cooper demonstrated that at sufficiently low temperatures such a state may be formed no matter how small the interaction due to the exclusion principle[1]. The Fermi surface is a constant energy surface in momentum space where all electrons of a given material at absolute zero occupy levels with energy less than the Fermi energy. Cooper demonstrated that electrons near the Fermi surface could form bound states mediated by a virtual phonon which assisted in the scattering of electron pairs. One electron would emit a phonon which would immediately be absorbed by another. The lowering of energy is greatest if the two electrons form cooper pairs having equal and opposite momentum and have opposite spins.

The presence of an attractive potential lowers the energy of an individual electron by an amount Δ. Thus at absolute zero all energy states will be occupied up to an energy E_f-Δ as compared to a normal metal where all states are occupied up to E_f. This leads to an energy gap in which a depairing energy equal to 2Δ must be applied to the Cooper pair before it can cross the gap. Normal resistivity is a result of electron-phonon collisions in which an electron is scattered according to energy and momentum conservation laws. A superconducting electron pair however has an additional binding energy which restricts the phonons which may be involved in a scattering event. Unless a phonon imparts an energy greater than 2Δ the pair will remain below the energy gap and will not be scattered. In high temperature superconductors the ratio $\frac{\Delta(0)}{E_f}$ is large, thus making thermal dissociation more difficult as compared to low temperature superconductors.

A many-electron wavefunction is constructed as a product of individual pair wavefunctions $\psi_i(r_1,r_2)$ which give the probability of finding Cooper pair electrons at r_1 and r_2. One main result of this formalism is that the Cooper pair coherence length is larger than the crystal lattice parameter. The coherence length is usually denoted by the symbol ξ_0 and is defined as the average distance between two electrons forming a bound pair. This means that at any given point in space the superconducting properties are governed by millions of other pairs centered within ξ_0 of the same location. BCS theory not only predicts the microscopic behavior of superconductors but also is capable of describing certain macroscopic phenomena such as superconductive tunneling. Ginzberg Landau theory reduces to BCS theory in the limit $T \rightarrow T_c$ [24]. It should be noted that the BCS model may not be applicable in detail to high temperature superconductors, but much of the language arising from the model is used to describe the behavior and properties of high T_c materials.

3.4 Type II Superconductors

Ginzburg-Landau theory predicts the existence of a superconducting state with a negative surface energy between superconducting and normal regions. The difference in free energy between a normal state and a superconducting state in zero applied field is $\frac{H_c^2}{8\pi}$, where H_C is the critical field at which the superconducting state is destroyed. Inside a superconductor, the free energy is lowered by an amount G_n-G_S due to the presence of superconducting electrons . This drop in energy is compensated by an increase in the free energy due to the change in magnetic field as it drops to zero some distance inside the sample. The free energy rises by an amount $\frac{H_c^2}{8\pi}$ if an external field Hc is applied. Due to these compensating terms, the free energy deep inside a superconducting sample is equal to the free energy of the normal region outside. At the superconducting-normal interface however, changes in energy are related to the penetration depth λ_L, and coherence length ξ_o of the superconductor as can be seen in the schematic diagrams shown in figure 3.1. Ginzberg-Landau theory predicts that if $\frac{\lambda_L}{\xi_o} < \frac{1}{\sqrt{2}}$ there will be a positive surface energy (type I superconductors) and if $\frac{\lambda_L}{\xi_o} > \frac{1}{\sqrt{2}}$ the surface energy will be negative (type II superconductors). The penetration depth λ_L is the distance a magnetic field penetrates into a superconducting sample before decreasing to 1/e its value at the surface. Therefore type I superconductors will try to minimize the surface area between normal and superconducting regions. On the other hand it is more energetically favourable for type II superconductors to increase the normal-superconducting interface area. They do this by allowing a number of normal cores to penetrate the sample. The normal cores are referred to as fluxoids or vortices due to the characteristic magnetic flux and circulating current associated with these objects.

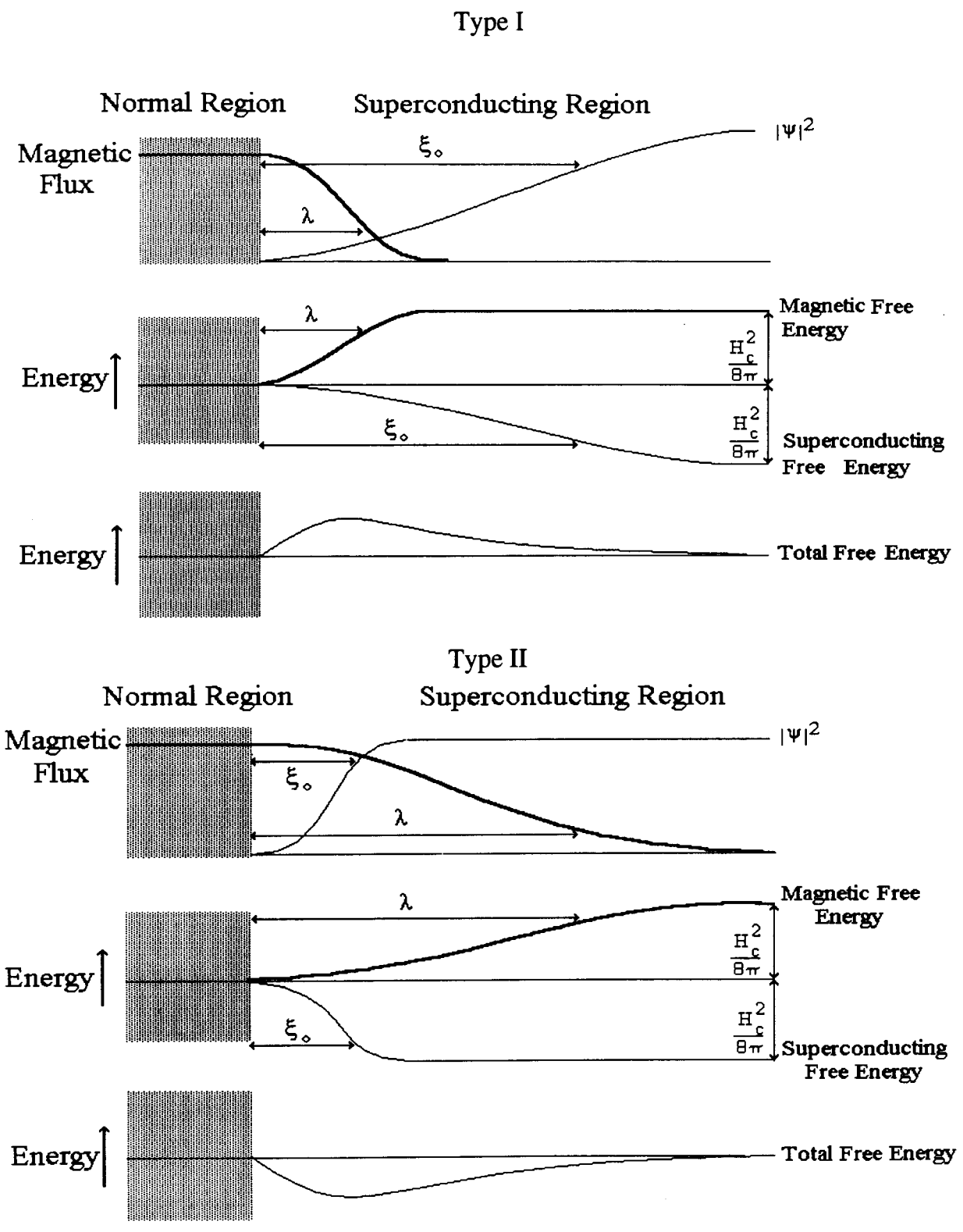

Figure 3.1 Origin of surface energy for type I and type II superconductors

If there is a negative surface energy or an extra demagnetization energy, superconducting regions may exist simultaneously with normal regions. Type I superconductors may exist in an intermediate state consisting of a mixture of superconducting and normal regions which are formed as a result of demagnetization effects. Due to this negative surface energy type II superconductors form a mixed state consisting of a regular lattice of normal cores threaded by magnetic flux surrounded by a vortex of superconducting current. The magnetic field associated with an isolated vortex extends a distance comparable to the penetration depth λ_L. Abrikosov first predicted such a state by solving the Ginzburg-Landau equations. He determined that a triangular lattice would be the most stable solution, this conclusion has been verified experimentally[2].

As a result of this vortex lattice superconductivity may be maintained with magnetic flux penetrating the sample. Regions exist in the material where the order parameter is still high, thus maintaining its superconducting character. The flux bundles or normal cores are formed initially at the edge of the sample where demagnetization factors are large ($H_{edge}>H_{c1}$). The flux bundles then experience a Lorentz force from supercurrents which are flowing around the sample screening the interior. This force pushes the fluxoids towards the centre of the sample. There exists another force due to pinning which opposes fluxoid motion towards the interior. In the static case where fluxoids are not moving

$$\frac{1}{c}\mathbf{J}\times\vec{\Phi}_o < \mathbf{F_p} \qquad (13)$$

where the first term is the Lorentz force and $\mathbf{F_p}$ is the pinning force acting on a flux line. When the pinning force exceeds the Lorentz force the vortices start to move and dissipate energy, thus the critical current is determined by the strength of the pinning centres.

If a field is applied perpendicular to the film, the field at the edge becomes higher than H_{c1} and vortices find it energetically favourable to enter the sample. The screening

current tries to exclude the external field. In the final state the current can not exceed J_c (see equation 13), this results in a partial penetration of magnetic flux. This behavior follows the rules of a critical state model[25]. For systems where the critical current is determined by the pinning force the critical state model may be described as follows. For any change in external magnetic field the film tries to maintain the previous magnetic flux distribution under the constraint that the current anywhere may not exceed J_c. It follows that magnetic flux is present in regions where the magnitude of the current has reached J_c.

In certain areas of device fabrication it is advantageous to operate with large currents. An example would be a superconducting magnet. Applied currents also move the vortices, which in turn causes an electric potential to be developed and results in energy dissipation. It is therefore necessary to provide a mechanism to prevent flux from penetrating from the edges. This is accomplished using various types of defects that provide a pinning force to oppose the flux motion. Some examples of pinning sites are impurities, sample edges, grooves, and indentations. Type II superconductors may exist in fields substantially larger than their type I counterparts. High Tc materials are exclusively type II which means that their study is relevant to applications.

As the applied field is increased the fluxoid density becomes larger. The distance between vortices is approximately

$$a = \left(\frac{\Phi_o}{B}\right)^{1/2} \tag{14}$$

where B is the macroscopic field that has penetrated the superconductor averaged over several vortices and Φ_0 is a flux quantum (=2.07 x 10^{-7} G cm^2). When the applied field first reaches H_{c1} vortices may penetrate and take up equilibrium positions at large distances from each other. The magnetic field associated with each will extend spatially a

distance governed by the penetration depth λ_L. The penetration depth λ_L follows the empirical relation

$$\lambda_L(T) = \lambda_L(0)\left[1-\left(\frac{T}{T_c}\right)^4\right]^{-1/2} \qquad (15)$$

Typically $\lambda_L(0)$ is on the order of 100 nm for type I superconductors, $Y_1Ba_2Cu_3O_7$ has a penetration depth of 150 nm as T approaches 0 degrees (the above equation varies slowly for $T<<T_c$).

The existence of an array of vortices has an effect on the magnetization of a type II superconductor. According to the Bean model[25] the density of vortices is a linear function of distance from the edge of the sample (superconducting cylinder in parallel applied field). The magnetization M of such a sample will be characterized as follows. In applied fields up to H_{c1} the magnetic field will be completely excluded giving a linear dependence of M with H. At H_{c1} fluxoids start to penetrate according to Beans model, this gives a quadratic polynomial dependence of M with H. This continues until the magnetic field has completely penetrated the sample giving a saturation magnetization. The critical current decreases with increasing magnetic field[26]. At high fields the critical current starts to decrease which in turn causes the magnetization to decline, eventually reaching 0 at H_{c2}. In the case of a thin film demagnetization factors create large fields at the edges which allow fluxoids to penetrate at applied fields much smaller than H_{c1}. The resulting magnetization can be approximated by the above description for a long cylinder except that the magnetic flux immediately penetrates the sample (H_{c1}=0). In the present experiment applied fields are small and the critical current may be taken to be constant, this results in a magnetization curve shown in figure 3.2.

According to equations 13 and 14 one might expect a fluxoid lattice with a lattice spacing of 2μm (at 5G) containing cores with a magnetic field spatially extending a distance comparable to the penetration depth (on the order of 0.1 μm). The garnet film

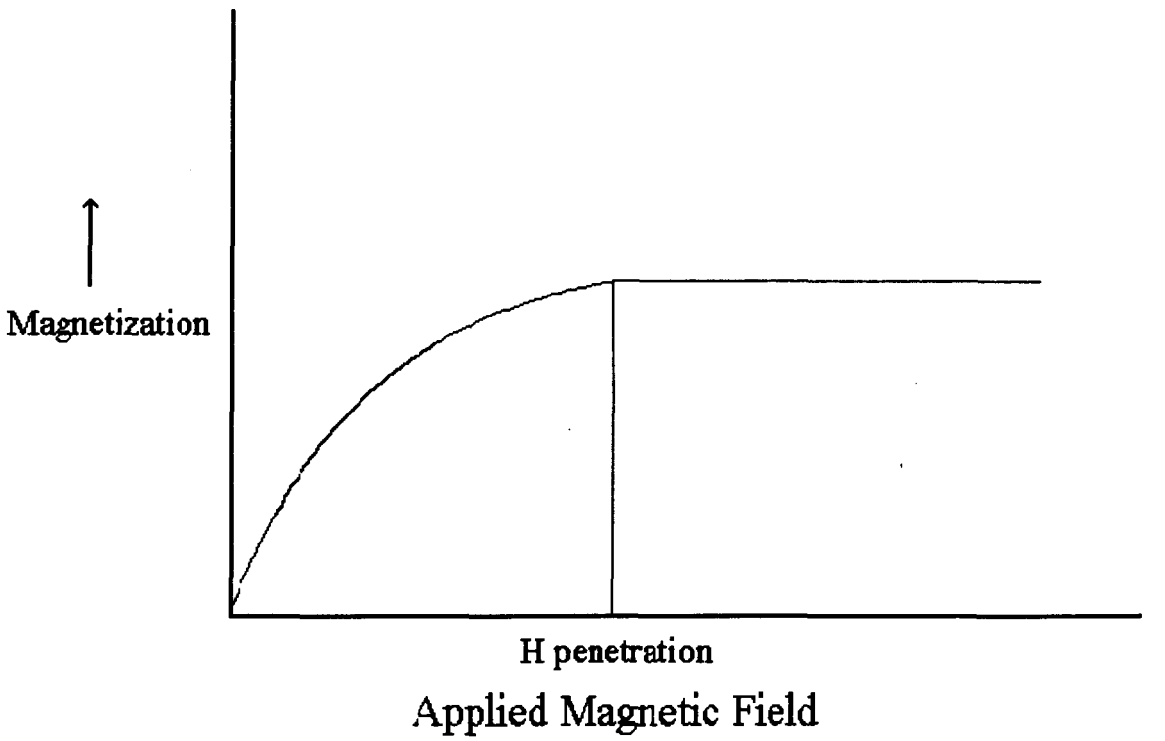

Figure 3.2 Schematic diagram of the magnetization of a type II superconducting cylinder as a function of an applied parallel magnetic field. This curve is based on Bean's model in a low applied field.

used in this experiment did not form magnetic bubble domains, but there do exist materials that permit bubble diameters of 1 μm. Provided that the bubble mobility is high enough it is conceivable that these might follow field gradients and tend to align with the fluxoid lattice. In memory devices bubble domains are moved using field gradients, caused by conducting layers placed on top of the garnet. The field gradients associated with a vortex might be capable of capturing moving bubbles. This would provide a method of imaging the vortex lattice at low fields where the distance between individual fluxoids is larger than the bubble domain.

Chapter 4

Imaging Flux Penetration in High Tc Superconductors Using Garnet Films

4.1 Introduction

The garnet film is used to image magnetic flux above the surface of a superconductor using the Faraday effect. The individual domains of the garnet film rotate polarized light by a specific angle depending on the magnetization and this angle is usually denoted by the symbol θ_f in units of $\frac{deg}{cm}$. The yttrium iron garnet is transparent in the visible spectrum and has a Faraday rotation of 0.024 $\frac{deg}{\mu m}$ (in the infrared, λ=1.2 μ m)[13]. This makes the visualization of domains possible by illuminating the garnet with polarized light and examining the reflected beam with an analyzer. Each type of domain (up or down) will rotate the polarization by $\pm\theta$. The analyzer may then be used to obtain a contrast between the domains. Domains magnetized in one direction will appear dark whereas those magnetized in the opposite direction will appear light. Figure 2.4 was obtained using this technique.

The garnet film consists of a series of strip domains magnetized perpendicularly to the surface. In zero field an equal number of domains are magnetized up and down giving a net zero average magnetization. Under the influence of an applied field the domain walls move enlarging those domains which are oriented along the applied field. The magnetic field will be proportional to the average magnetization. If a field is applied in the direction of the dark domains the entire film will appear to become darker as these domains expand and the light domains contract. A field applied in the opposite direction to the dark domains will cause the entire film to become lighter. The strength of the field

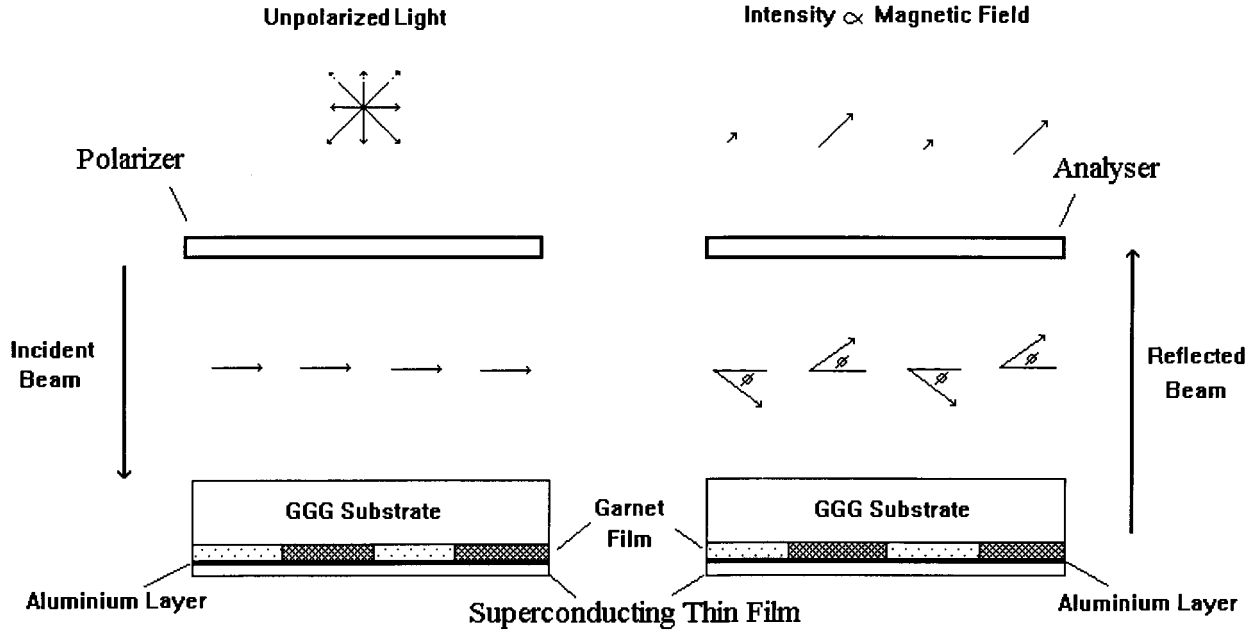

Figure 4.1 Faraday rotation in a garnet film in zero applied field. This is a side view of the garnet film, the magnetic field is applied perpendicular to the surface. The shading represents different domains in the garnet film. Each domain rotates the polarization in a different direction.

at a particular position is obtained by averaging the light intensity over a region around that point (the region has to be larger than the width of the strip domains).

A CCD camera (Loral Fairchild CAM/CCD5000) was used to capture images of the garnet. It consists of an array of 483 x 378 sensing elements which record light intensity. The domains of the garnet used in the present investigation are approximately 10μm wide in zero applied field at 77 K. This implies that the domain structure will not be resolved when imaging objects approximately 1 cm x 1 cm (500 pixels x 20 μm = 1cm). The intensity of light falling on each pixel will correspond directly to a magnetic field strength.

4.2 Experimental Setup

The garnet film must be used with reflected light as it is placed on top of a superconducting film that is usually opaque or highly absorbing. Thus polarized light is transmitted through the garnet film, is rotated according to the magnetization of the domain and is then reflected from a aluminum layer placed between the superconductor and garnet as shown in figure 4.1. The light is further rotated on its exit path from the film and is then passed through an analyzer to obtain a contrast between the two domain magnetizations. The resulting intensity is averaged over several domains to give a value which represents the strength of the local magnetic field.

The reflective coating of aluminum was evaporated on to the yttrium iron garnet film (taking care to evaporate the aluminum on the YIG as opposed to the GGG). Varying amounts of aluminum were used until a coating was found that would provide a highly reflective layer which would not peel off. The thickness of the layer is estimated to be 1000 Angstroms (2 cm^2 of ordinary aluminum foil was placed in the evaporation cup, the cup was approximately 13 cm from the garnet film).

The experimental setup is shown in figure 4.2. The garnet film was placed on top of a flat superconducting sample and the domain pattern of the garnet was examined. The

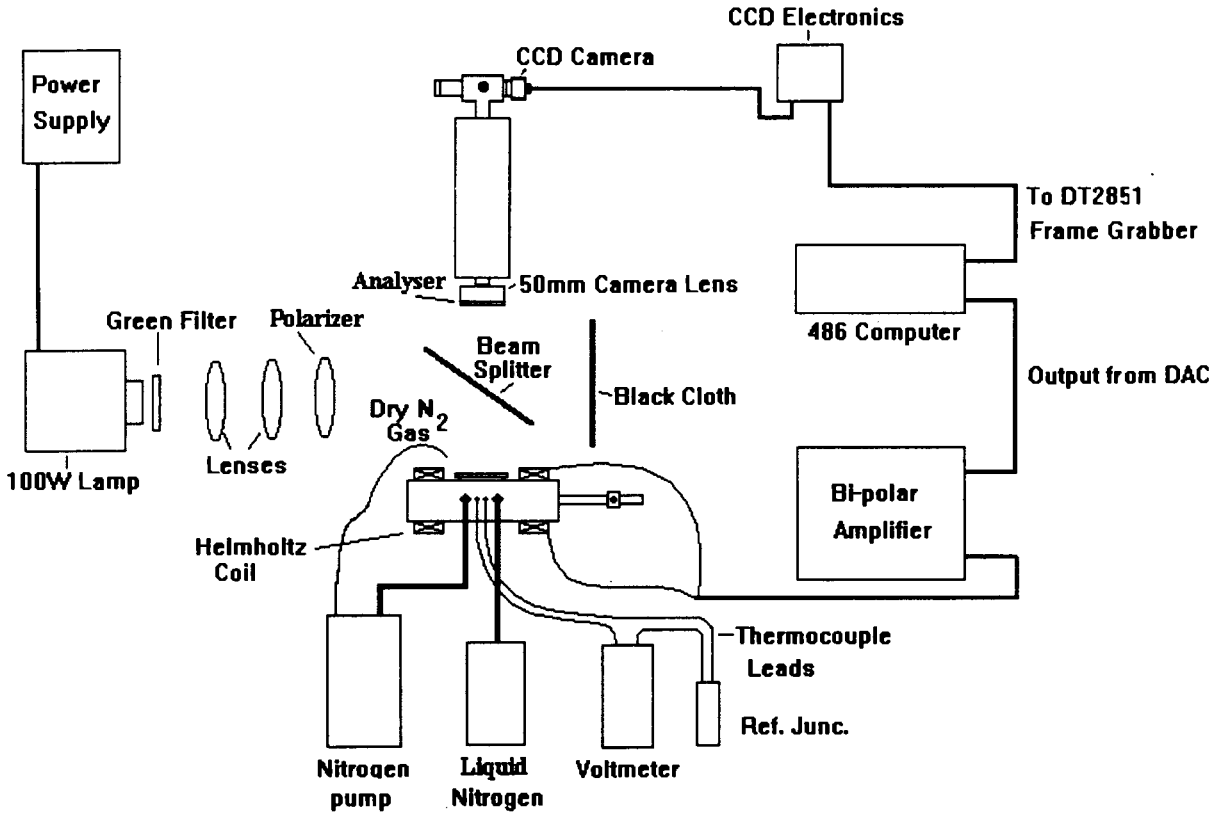

Figure 4.2 Experimental setup. The Helmholtz coils shown above produce a uniform field perpendicular to the surface of the sample.

superconducting sample is thermally anchored inside an optical dewar on a hollow copper block which is filled with liquid nitrogen. Images are captured using a Lorel Fairchild CCD camera and a Data Translation 2851 frame grabber and may be subsequently averaged to reduce noise. The images obtained are represented on a 256 greyscale where a dark shade depicts a large field perpendicular to the film and a white shade represents the same field in the opposite direction.

The measurement of superconducting properties using a magneto-optical technique required the construction of an optical dewar capable of operating at 77K. The construction of this device was based on a commercial dewar produced by Linkham Scientific Instruments. A top view of the dewar is shown in figure 4.3. The materials used were aluminum and brass with the exception of the nitrogen lines which were stainless-steel.

Nitrogen is pumped from a separate dewar through a filter to prevent ice entering the system. It is pumped through a small tube surrounded by an insulating material to the optical dewar. This tube is inserted into the hollow copper block shown in figure 4.3 which fills with liquid nitrogen. The dry gas which boils off is sucked into the pump and may be used to clear the cover glass from condensation which may arise during experimentation. The system is first evacuated using a small roughing pump. When the valve shown in figure 4.3 is closed the vacuum inside prevents condensation of water from the air inside the chamber. Condensation makes it impossible to obtain clear images.

A non-magnetic thermocouple (copper-constantan) was soldered to the copper block and wound several times around the circumference to prevent conduction of heat from the thermocouple leads outside the dewar to the junction.

The superconducting film is thermally anchored to the copper block using a silicon based grease, and the garnet film is placed on top of the superconducting sample (aluminum side down).

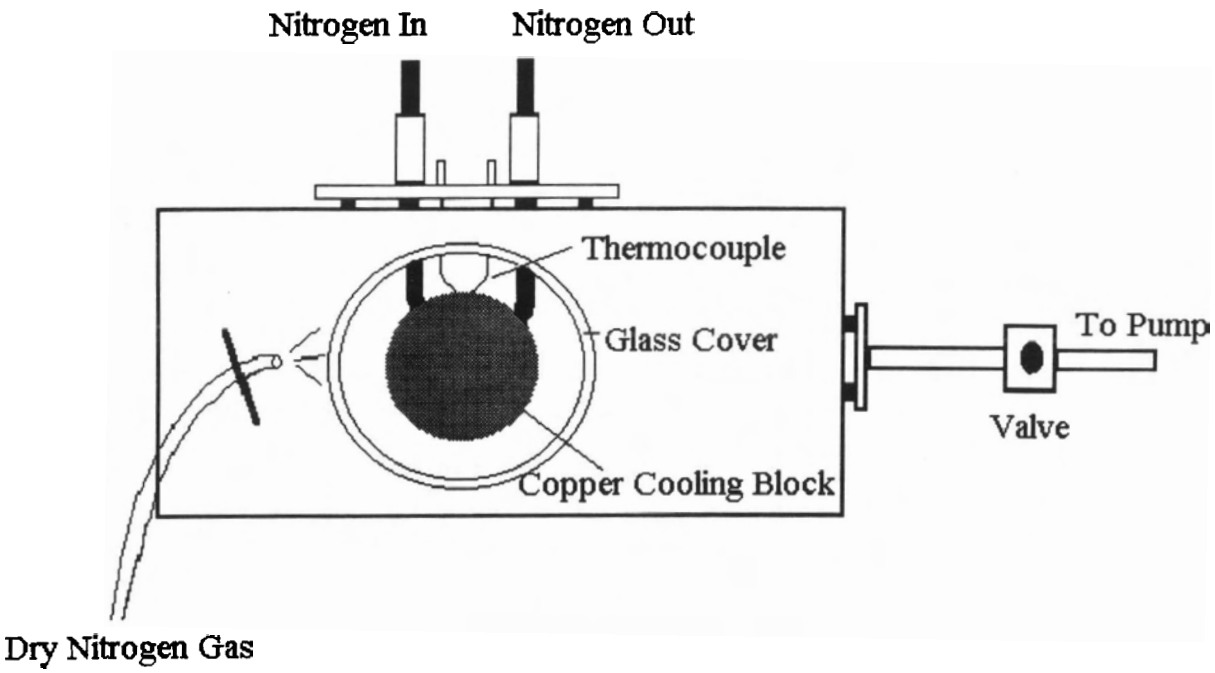

Figure 4.3 Top view of optical dewar. The sample sits on the Copper block.

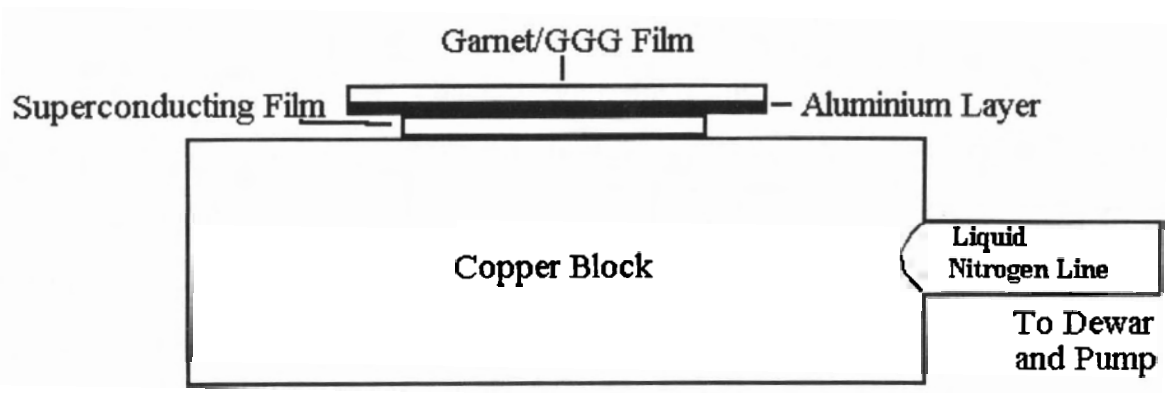

Figure 4.4 Side view of sample Installation.

The cooling stage is placed between two Helmholtz coils connected in parallel. The coils are operated remotely by a 486DX-33 computer equipped with a digital to analog converter. The computer controls the current flowing through the Helmholtz coils by providing a signal -5 to +5 V which is fed through a Kepco bi-polar amplifier to the coils. Currents up to 14 amps were applied to these Helmholtz coils. They were found to produce 14 Oe/Ampere in the area of the mounted sample.

A 100 W lamp was used in conjunction with a system of condenser lenses to maximize the light intensity falling on the sample. A green filter was found to provide an optimum contrast. The garnet film has a large Faraday rotation at this wavelength[14], and the CCD has a maximal spectral response. The beam passes through a polarizer and is subsequently reflected onto the sample by a beam splitter. The beam splitter allowed a percentage of the incident light to pass through and reflect from objects directly behind the beam splitter. Frequently while working around the experiment, a hand or body placed in the transmitted beam would reflect light back at the beam splitter and up into the CCD camera. It was necessary to use a black screen to prevent this diffuse reflection from re-entering the optical system. The light beam passes through the garnet, the polarization rotates according to the domain through which the beam passes, reflects from the aluminum layer, and passes back through the beam splitter into a 50 mm camera lens fitted with a Polaroid filter (as previously discussed in section 4.1). The 50 mm lens is attached to an adjustable stand which allows the image to be focused onto the CCD. The stand is also designed to allow the image to be magnified by varying the distance between the camera lens and CCD. It is also possible to replace the 50 mm lens with a microscope objective to achieve a higher magnification.

The CCD outputs a standard RS170 video signal, 483 pixels by 378. The gain and offset may be controlled to optimize the contrast. The video signal is captured by an IRIS DT2851 frame grabber card and the image is stored on a computer disk. Several

computer programs were written to acquire, then average and display the data. An example is included in appendix A.

4.3 Experimental Procedure

The superconducting samples were cooled to 77K in the presence of the earth's magnetic field. A computer program was written to control various magnetic field strengths and to acquire images. The magnetic fields were applied perpendicular to the sample.

The procedure is limited by the field which causes domains magnetized opposite to the applied field to collapse leaving the garnet in a saturated state with one domain in the same direction as the applied field (the garnet film used in this experiment experienced domain collapse at ≈30 Oe). Above this value the domain structure undergoes large discontinuous jumps until the entire film is magnetized in one direction. This is evident in a few images where the flux front is prematurely clipped.

In order to maximize the light intensity falling on the sample the light source was placed approximately 1m away from the beam splitter. Thus the light did not consist of perfect plane waves and caused an illumination intensity that distorted the image of the magnetic field. It is therefore necessary to subtract the background intensity. The background may be subtracted in two different ways. A zero field image may be used for the background subtraction. Upon reversing the field the observed pattern was inverted but spatially identical. Thus subtracting two images in an applied field (taken with the field at the same strength but in opposite directions) the background illumination may also be reduced. If the background illumination is very non-uniform the images may also be divided by the background. This was not necessary when using a microscope objective as the background illumination was fairly uniform. This is due to the smaller solid angle of the wave front used by the objective (as the scale becomes smaller the light is more planar). A cross section of the background intensity for the 50 mm camera lens is shown in figure 4.5.

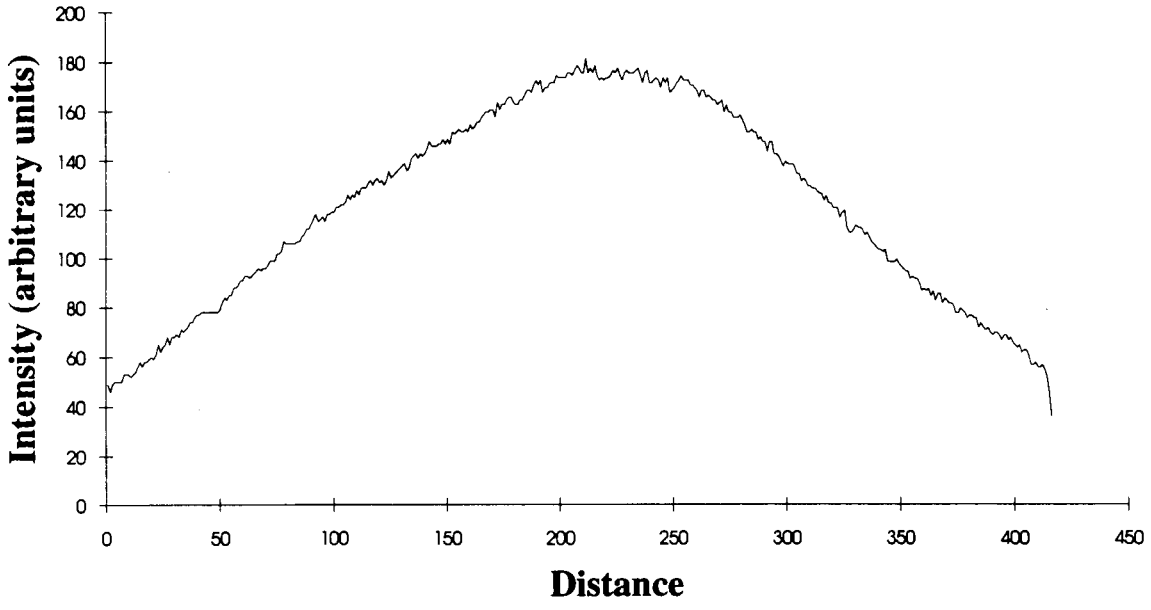

Figure 4.5 Background Illumination Intensity (arbitrary units) vs. Distance (this cross section corresponds to approximately 1cm)

Two methods were used in acquiring data.

(A):The superconducting film in an applied field.

The magnetic field is applied at a specific strength, the image is taken with the field still on. The field is then reversed and another image taken. These two images are subtracted so that only changes due to the magnetic field are visible and the background illumination is reduced.

Figure 4.6 shows a schematic of the trapped magnetic field inside a superconductor based on the Bean critical state model[25]. A positive field is applied perpendicular to the film and the resulting image is captured (shown by the top line). The field is reversed and another image is captured (shown by the middle line). These two states are then subtracted leaving an image represented by the bottom line.

(B)The film in a remnant state.

As opposed to method A, where images were taken in the presence of an applied field, method B images the superconductor in its remnant state. The remnant state is defined as the magnetic field distribution of the superconductor in the absence of an applied field after subjecting the film to a field perpendicular to its surface.

In this method, the field is applied for a short period of time at a specific strength, H, then it is turned off and an image is taken. The field is then reversed to -H, it is then switched off and another image is acquired. The images are then subtracted. As mentioned previously the field distribution due to the application of opposite fields are spatially equivalent but inverted.

The procedure in both methods can be repeated several times and the results averaged to reduce noise. Typically 128 images were taken, reducing random noise by a factor of 10. The image files are scaled to a 256 greyscale by subtracting from each

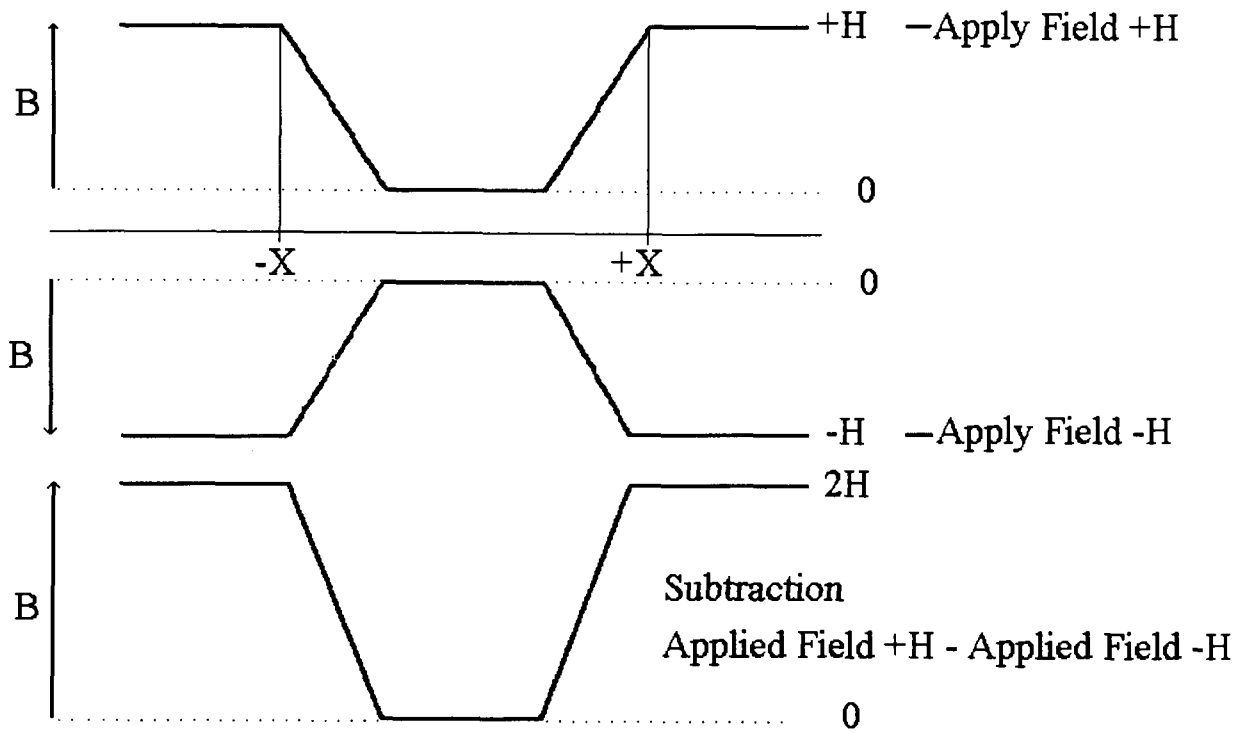

Figure 4.6 Procedure used to obtain an image in an applied field (H). The magnetic field profile inside the sample B, is based on a long cylinder in a parallel magnetic field. B represents the field strength in the direction of the cylinder. The sample is located between -X and +X.

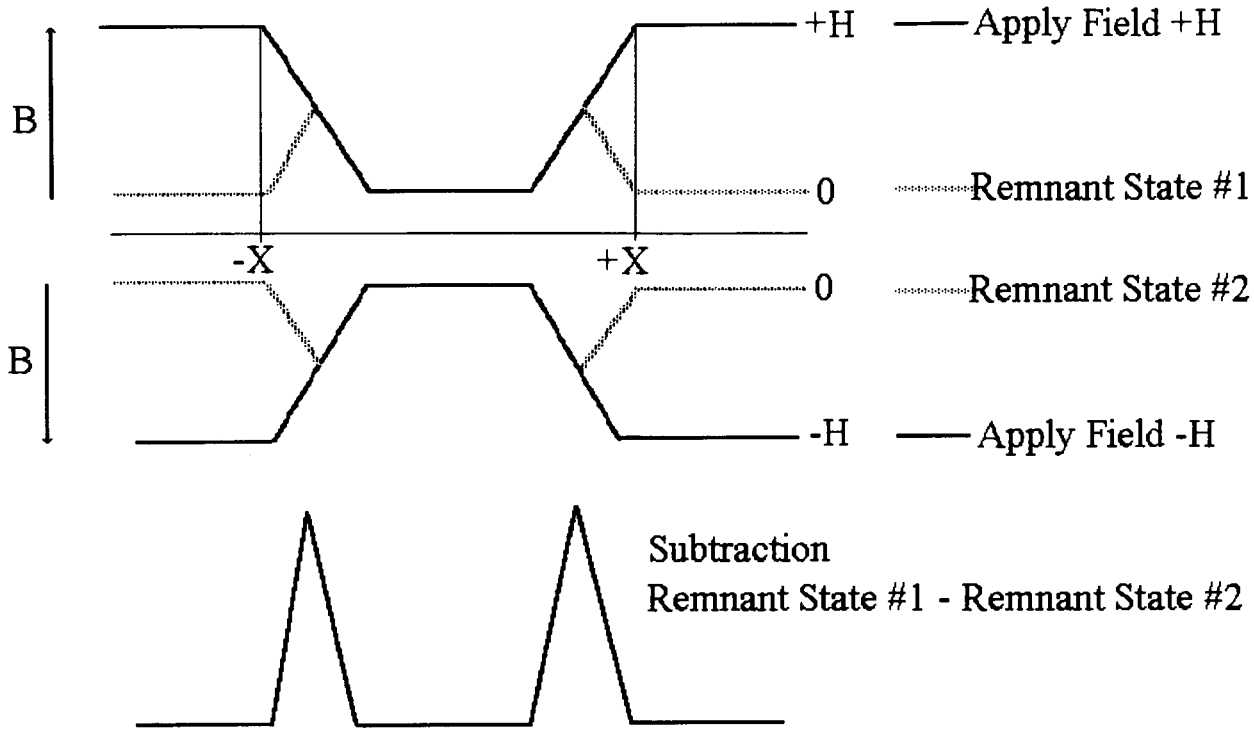

Figure 4.7 Remnant state after applying a small field (H). The magnetic field profile inside the sample B is based on a long cylinder in a parallel magnetic field. B represents the field strength in the direction of the cylinder. The sample is located between -X and +X.

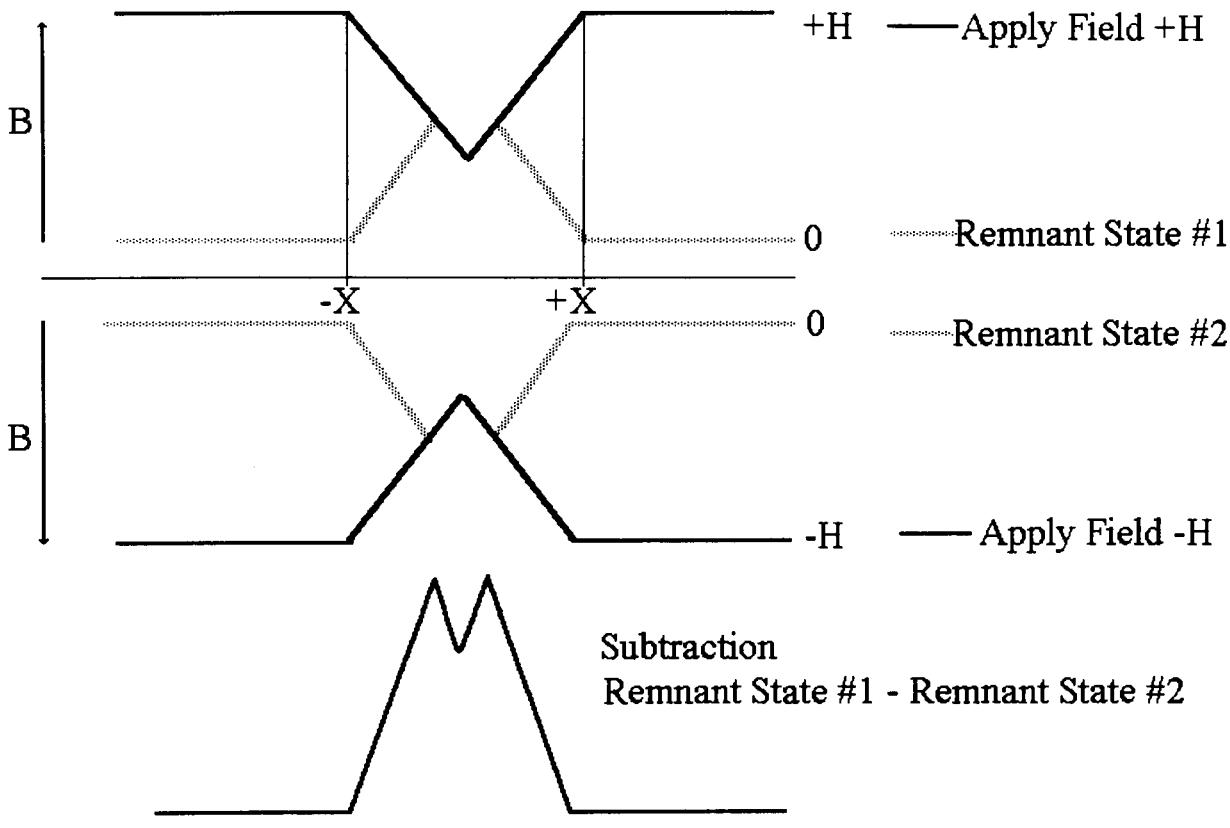

Figure 4.8 Remnant state after applying an intermediate field (H). The magnetic field profile inside the sample B is based on a long cylinder in a parallel magnetic field. B represents the field strength in the direction of the cylinder. The sample is located between -X and +X.

pixel the minimum intensity then dividing that result by the maximum and multiplying by 256.

Taking data in the remnant state offers a few advantages over the applied state. When a field is applied to the sample it shields the interior while leaving the periphery with a value equal to the applied field as shown in figure 4.6. When taking an image of the remnant state the field is turned off and the flux around the outside of the sample leaks out as shown in figure 4.7. Therefore the fields depicted in the remnant images are approximately half as large as the corresponding applied field images. This allows the garnet film to operate in the linear region for a greater range of field strengths.

There are several possible sources of noise. The Helmholtz coils can induce currents in the copper cooling block thus warming our sample. The drift in temperature was found to be approximately one degree on applying and removing a 40 Gauss field. The noise associated with this effect would grow rapidly as the temperature approaches T_C and J_C falls to 0. Heating the sample through infra-red radiation from the light source was also a concern, but this effect was negligible due to the substantial amount of glass between source and sample.

The optical bench used to secure the components of the experiment was made from steel and was ferro-magnetic. This had a noticeable effect on the field produced by the Helmholtz coils. The field differed by a couple of percent when measured above the bench compared to a measurement far away from the bench. Future experiments will be carried out at a larger distance above the bench or with an aluminum bench.

Other possible sources of noise include stray fields inside the computer interfering with the frame grabber, and a non-uniform magneto-optical cover glass.

As previously stated, the garnet film exhibits linear behavior in low fields while becoming increasingly non-linear at larger fields. Several hysteresis loops were obtained for different field ranges. After taking care to remove any grease on the cooling block the garnet was mounted inside the dewar. The garnet was cooled to 77 K and 3 hysteresis

loops were taken, as shown in figure 4.10. This was done to mimic the conditions under which the garnet was used during normal operation. Each point represents the sum of intensities over an entire image. The graphs are an average of 10 passes around the loop.

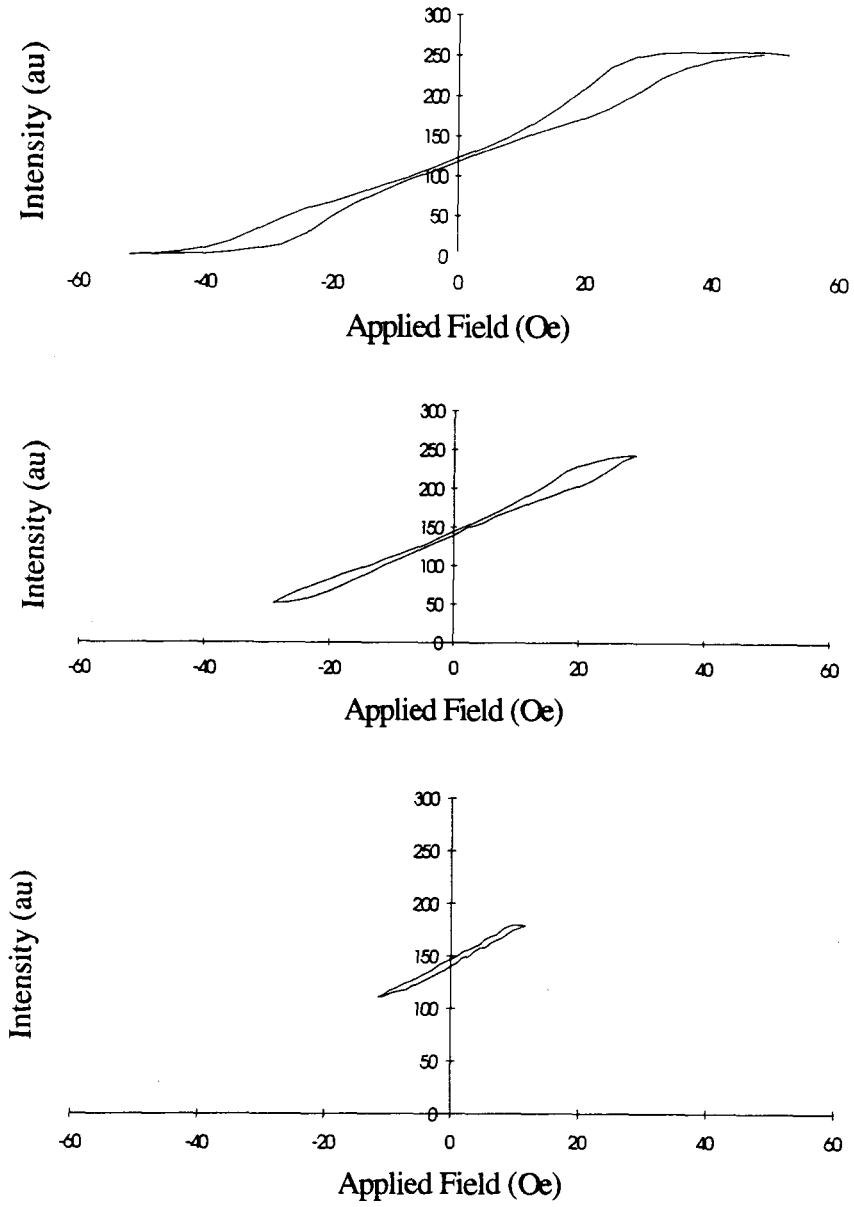

Figure 4.10 Three magnetization hysteresis loops of garnet film taken at 77 K. As a rough calibration each graph was scaled to the same greyscale range as the images, 0-256 (provided that the garnet has saturated in some part of the picture). Intensity is given in arbitrary units (au). Each graph was acquired under slightly different lighting conditions, and was scaled by the same factor as the top graph, therefore the intensity scale of each loop in relation to the others is only an approximation.

Chapter 5

Results and Discussion

5.1 Current Distributions

This section describes a method by which a current distribution may be obtained from the magnetic field measured above the surface of a thin film. The current may be written in terms of a magnetization which is directly related to the measured field. All calculations are done with a coordinate system in which x,y are in-plane coordinates while z is the height above the film. The thickness of the film is denoted by d.

The macroscopic relation $\mathbf{J} = c\nabla \times \mathbf{M}$ allows the current distribution to be expressed as a function of the magnetization. The following equation gives the surface current density (statamps/cm) associated with an area of the film $(\Delta l_X)(\Delta l_Y)$ in terms of the appropriate magnetization gradients.

$$\frac{1}{c}\mathbf{J} = \frac{\partial M_z}{\partial y}\hat{\mathbf{x}} - \frac{\partial M_z}{\partial x}\hat{\mathbf{y}} \approx \frac{\Delta M_z^y}{\Delta l_y}\hat{\mathbf{x}} - \frac{\Delta M_z^x}{\Delta l_x}\hat{\mathbf{y}} \qquad (1)$$

The superscripts on ΔM_Z denote in which direction the partial derivative is evaluated.

The vertical component of the external field B_Z may be written in terms of the circulating currents using the Biot-Savart law. The term magnetic field will refer to the magnetic induction, everywhere except cases where a distinction between H and B is necessary. The following equation gives the contribution to the total field due to a volume current density **J** (statamps/cm^2).

$$\mathbf{B} = \frac{1}{c}\int \frac{\mathbf{J}\times\mathbf{r}}{r^3} dv \qquad (2)$$

The vector **r** denotes a vector between the current element and a position P at which **B** is calculated. This is equivalent to a surface current integral times the thickness d. Transforming this surface integral to a 2 dimensional sum (d times Δl^2 and summing up surface current densities) and assuming the current element is at a distance $|\mathbf{r}|$ $\mathbf{r} = x\hat{\mathbf{x}} + y\hat{\mathbf{y}} + z\hat{\mathbf{z}}$, gives the z component of the magnetic field

$$B_z(P) = \frac{d\Delta l^2}{c} \sum_{i,j} \frac{J_x(i,j)y - J_y(i,j)x}{r^3} \tag{3}$$

This in turn may be written in terms of the magnetization by substituting equation 1. If one assumes a square current element $\Delta l_X = \Delta l_Y = \Delta l$ then

$$B_z = d\Delta l^2 \sum_{i,j} \left(\frac{1}{\left(x^2 + y^2 + z^2\right)^{\frac{3}{2}}} \right) \left[\frac{\Delta M_z^y(i,j)}{\Delta l} y + \frac{\Delta M_z^x(i,j)}{\Delta l} x \right] \tag{4}$$

If we assign a square two dimensional grid (N x N) to the magnetization we may calculate the vertical component of the magnetic field at a point (m,n) on that grid by summing up equation 4 over i and j with x and y defined as

$$x = \Delta l(m-i-1/2) \qquad y = \Delta l(n-j-1/2) \tag{5}$$

The grid used to calculate the magnetic field is shown in figure 5.1. The vertices of the grid represent values of magnetization and measured field while dots represent positions of current elements.

Using the definitions given above, the magnetization at a point (m,n) in a 2-dimensional grid due to all small current elements may be expressed with appropriate indices as

$$B_z(m,n) = d\Delta l^2 \sum_{i,j=1}^{N} \frac{[M(i,j+1) - M(i,j)](n-j-1/2) + [M(i+1,j) - M(i,j)](m-i-1/2)}{[(m-i-1/2)^2 \Delta l^2 + (n-j-1/2)^2 \Delta l^2 + z^2]^{3/2}} \tag{6}$$

The geometry of the sample then determines a system of linear equations $\mathbf{G} \cdot \mathbf{M} = \mathbf{B}$ where **G** is an N^2 x N^2 matrix of coefficients determined by the geometry, **M** is an N x N matrix representing the magnetization and **B** is an N x N matrix representing the measured vertical component of the field above the sample. The magnetization can thus be calculated from measured B_Z values by solving the system of equations. The current distribution can then be determined using the magnetization.

This system of linear equations was solved for a thallium based high T_C film after it was subjected to an applied field of 20 Oe. The magnetic field shown in figure 5.2 was measured in zero applied field (a remnant state) at the surface of the sample, z=0. The resulting magnetization is shown in figure 5.3, note that it closely resembles the vertical component of the measured field. The currents will flow along lines of constant M, $\mathbf{J} = c\nabla \times M_z \hat{\mathbf{z}}$ is normal to ∇M_z which is by definition normal to a contour plot of M. A contour plot of the magnetization gives the current distribution and is shown in figure 5.4. The magnitude of the current is equal to the magnitude of the curl of M. This leads to the current distribution shown figure 5.4, it contains four closed current loops, a larger loop flowing around the periphery and a smaller loop close to the centre which flows opposite to the current at the edge.

The magnetic field data used to obtain figures 5.3 and 5.4 was not calibrated, therefore these images only provide a qualitative description of the current distribution. It was found that the application of boundary conditions was unnecessary as the measured field distributions caused the magnetization to fall to zero outside the film.

The measured magnetic induction outside the sample is equal to the vertical component of the magnetic induction inside the sample. Applying appropriate boundary conditions at the sample surface one obtains,

$$\mathbf{H}_{out} = \mathbf{B}_{out} = \mathbf{B}_{in} = \mathbf{H}_{in} + 4\pi\mathbf{M} \qquad (7)$$

Application of Maxwell's equation $\nabla \times \mathbf{B} = \frac{4\pi}{c}\mathbf{J}$ and using $\mathbf{J} = c\nabla \times \mathbf{M}$ leads to a magneto-static equation,

$$\nabla \times \mathbf{H}_{in} = 0 \qquad (8)$$

Analysis of Hall probe data [3] has revealed that the magnetization is orders of magnitude larger than the external field $\mathbf{B_{out}}$ and is topographically similar. This also implies that H_{in} is large and $H_{in}^z \approx -4\pi M$.

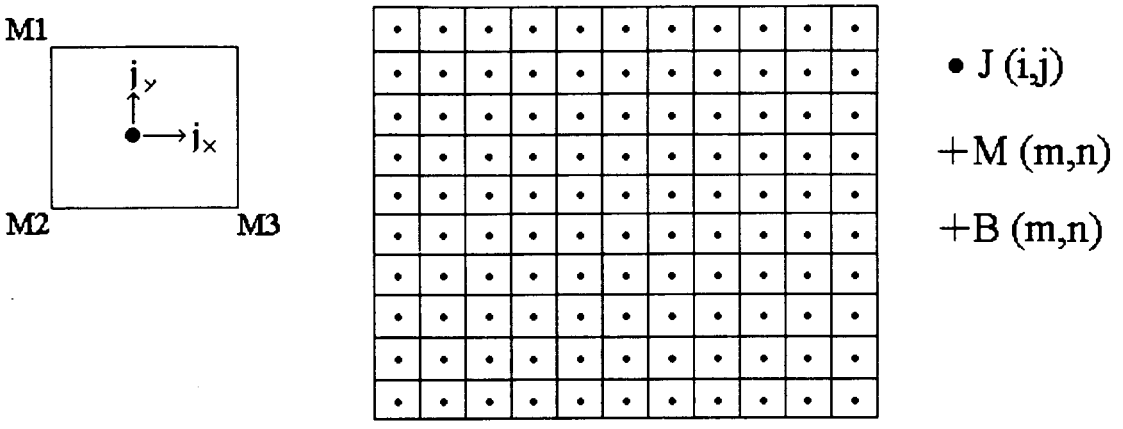

Figure 5.1 Section of 2-dimensional grid used to calculate current distributions. The magnetization and measured field are given points at the vertices of the above grid. The current elements are centred on points marked by circles and are defined by the scheme shown on the right, $j_X=\frac{c}{\Delta l_y}$(M1-M2) and $j_Y=\frac{c}{\Delta l_x}$(M3-M2). The current filament is located at i+1/2, j+1/2.

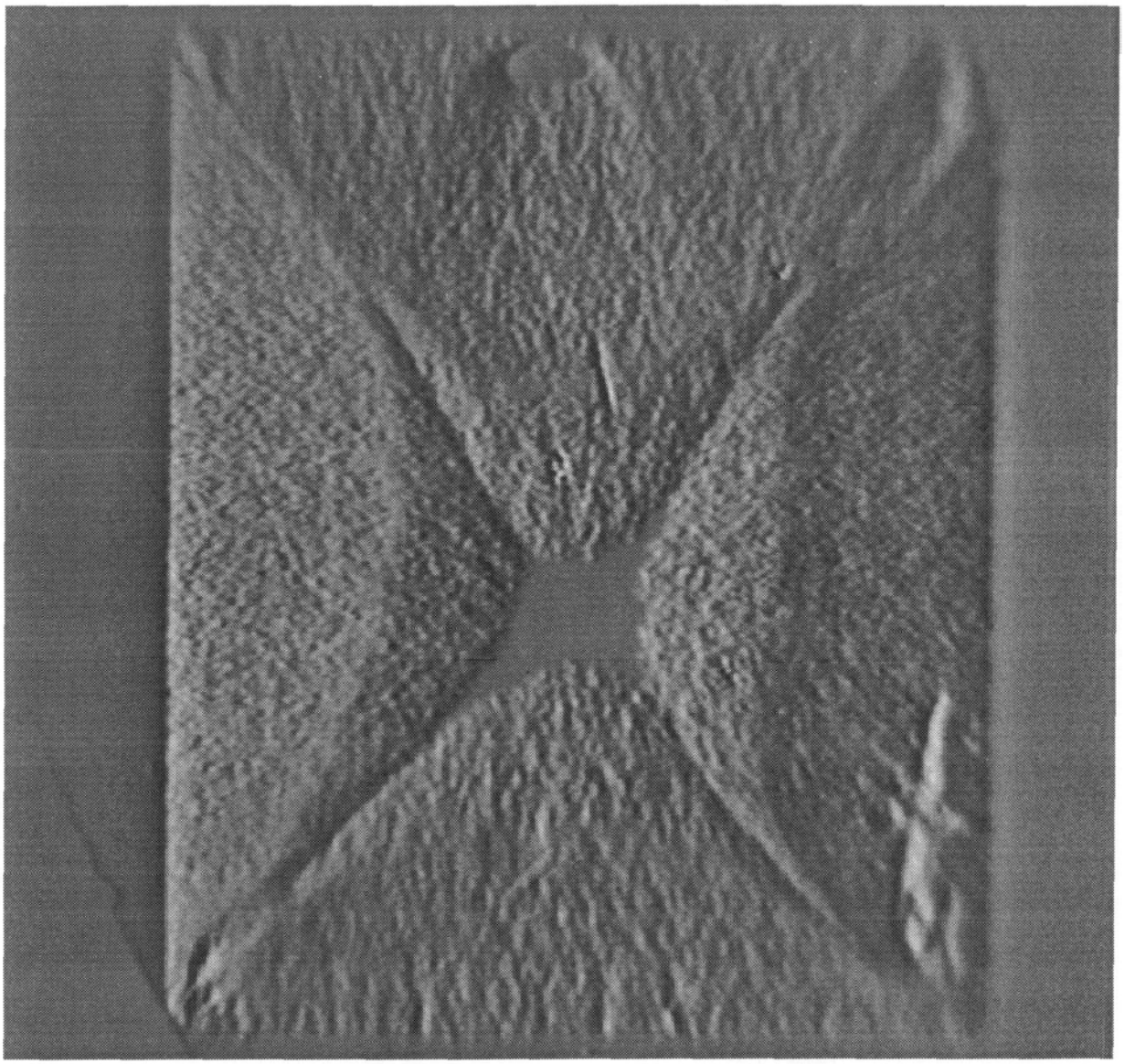

Figure 5.2 Shadowed image of a remnant state after the application of a 20 Oe field. The magnetic field is zero in the centre of the film, it gradually rises to a maximum half way towards the edge. It then decreases, turning negative close to the edge (due to demagnetization effects) and levels off to zero far away from the film.

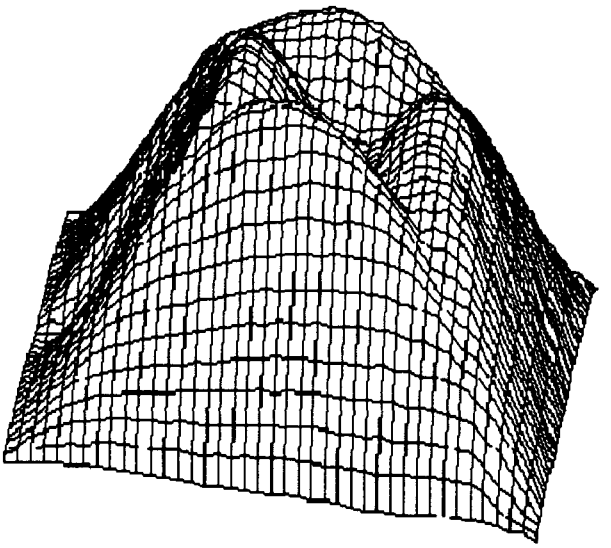

Figure 5.3 A magnetization plot of the 20 Oe remnant state of a thallium based film

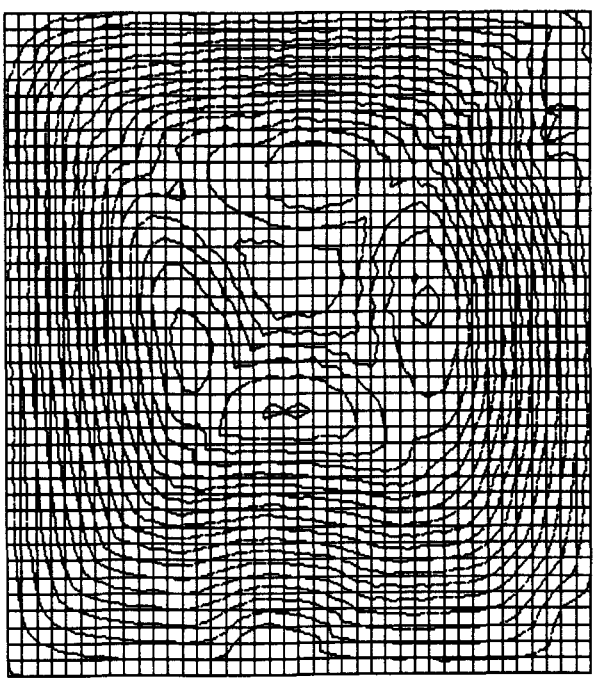

Figure 5.4 Contour plot of the magnetization plot of figure 5.3 representing the current distribution. The magnitude of the current is equal to the magnitude of the curl of M.

To estimate the order of magnitude of M one may assume that in a remnant saturated state (where the current everywhere is critical and flows approximately in a square around the sample) M(x,y) approximately forms a pyramid like structure. In this case the magnetization is a linear function of distance rising to a maximum in the centre of the film with a slope given by $\mathbf{J} = c\nabla \times \mathbf{M}$. Assuming a sample 1 cm across and a critical current density of $J_C=10^6$(amps/cm^2), this gives

$$M_{max} = \frac{1}{2} cm \cdot \frac{J_c}{c} = (\frac{1}{6\times10^{10}} s)(3\times10^{15} \frac{StatAmps}{cm^2}) = 5\times10^4 Gauss \qquad (10)$$

$$4\pi M_{max} \approx 6\times10^5 Gauss$$

This value is orders of magnitude higher than the measured magnetic field, this may be explained by demagnetization factors inherent to the geometry. The magnetic field is being greatly altered by a very thin (negligible volume) film.

The magnetic profiles obtained in the present study indicate that current flows in characteristic patterns (determined by geometrical factors), that try to maintain the flux distribution under changing magnetic environments. In all, three distinct patterns were observed in the square film samples that were studied. A square current distribution flowing around the periphery of the film has been observed (figure 5.4). In low fields, remnant state images have revealed currents flowing in several closed loops, again refer to figure 5.4. There is also evidence that a small current loop flowing opposite to the general screening currents exists in the centre of the film (in a remnant state). The remainder of this section will be devoted to presenting the experimental conditions that result in these characteristic current profiles.

The images in figure 5.5 show the remnant state of a thallium sample with a relatively low critical current density. A low critical current density is ideal for producing images with the garnet film used in this experiment. Superconducting films with a low critical current density allow flux to penetrate further into the sample because screening currents are not very large. This allows the garnet to operate without saturating.

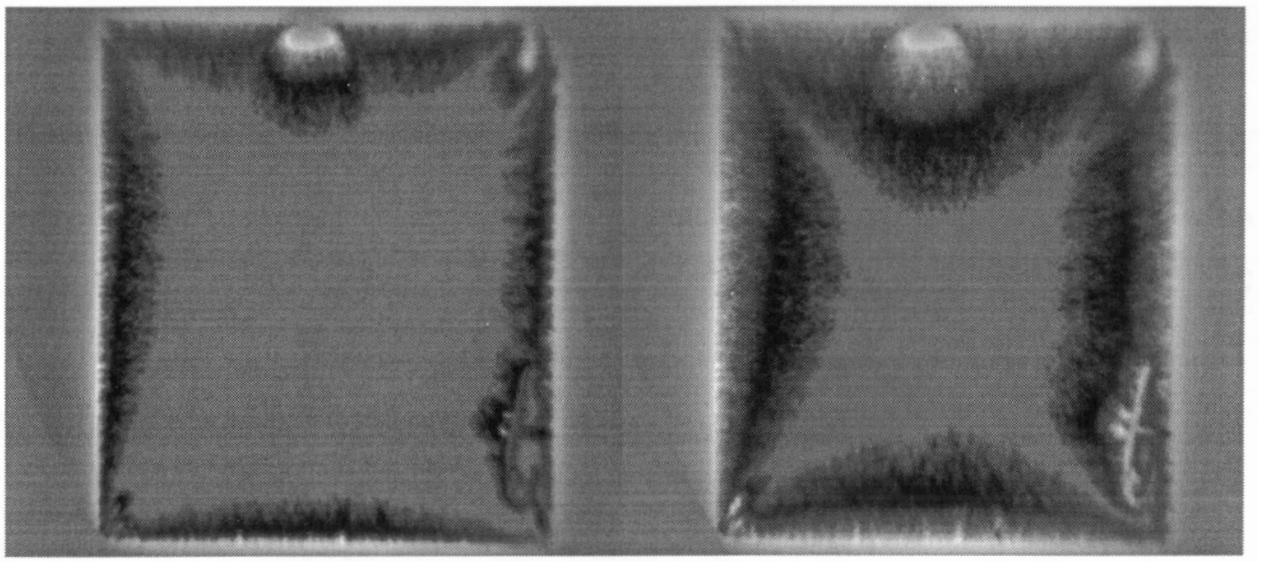

5 Oe 10 Oe

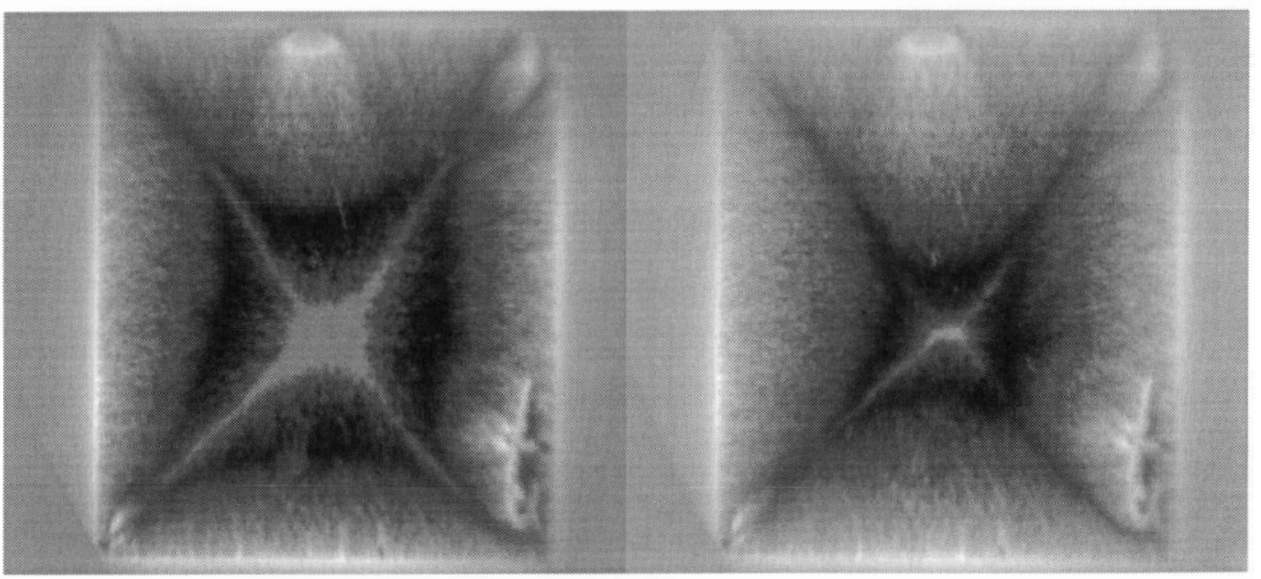

20 Oe 30 Oe

Figure 5.5a Sequence of images representing the remnant state of a thallium based film after application of the specified field (5-30 Oe). Note the change in contrast of the cross like structure between 20 and 30 Oe.

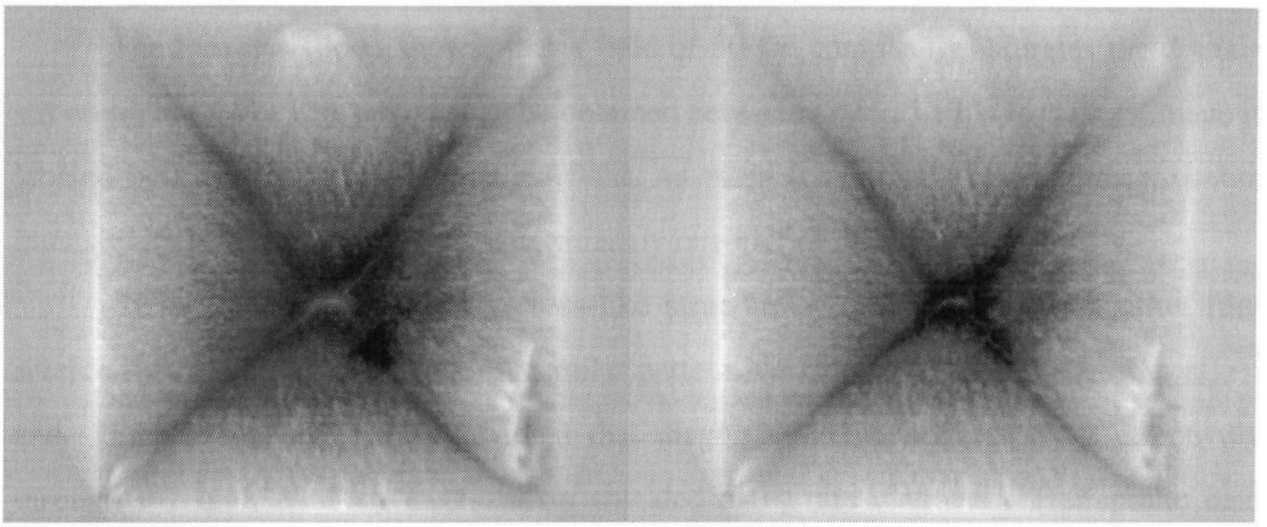

40 Oe 50 Oe

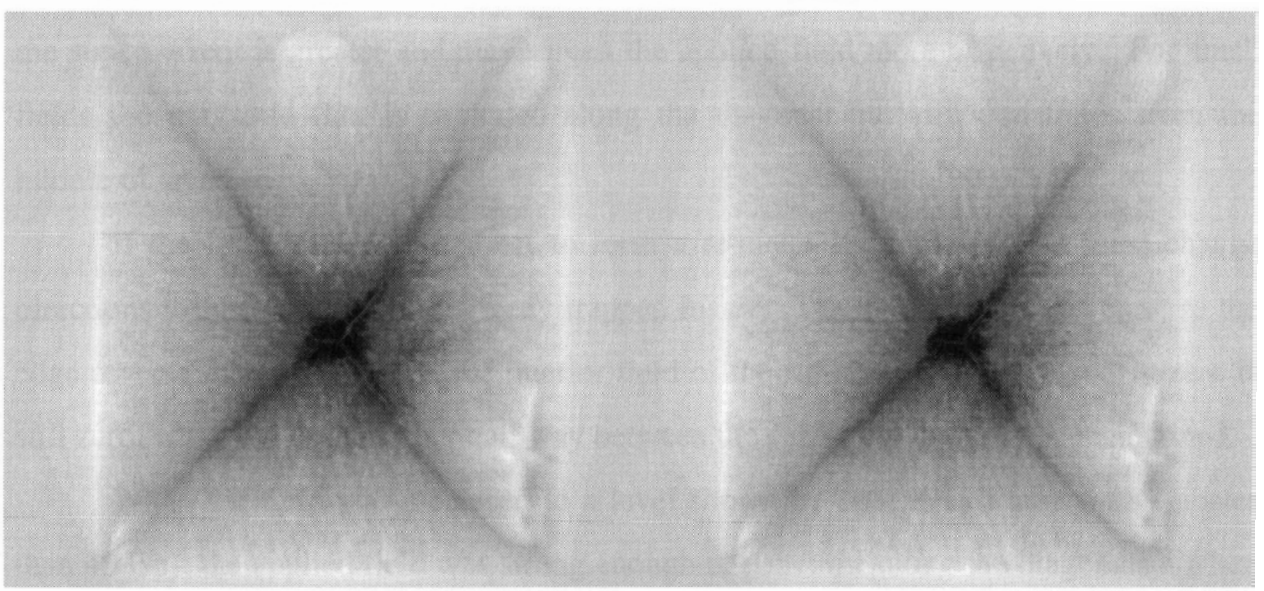

75 Oe 100 Oe

Figure 5.5b Sequence of images representing the remnant state of a thallium based film after application of the specified field (40-100 Oe). The dark cross shown in these images is a maximum where shielding currents trap flux more effectively. Also evident is a small region in the centre where a minimum exists for large fields.

The hysteresis loop shows that a field of 30 Oe completely saturates the domain structure, but a linear response may be obtained between -20 and +20 Oe. Each image is labeled by the strength of the applied field. As these are remnant states, the maximum intensity in these images will be approximately one half of the applied field.

Evident in the images is a cross-like structure where the superconducting film shields flux along the diagonals. A similar pattern has been reported by Brull et al. [27] and Huebener et al.[9] . It is evident that magnetic flux penetrates more effectively through the middle of an edge and is shielded along the diagonal. Hall probe data indicates that although the current mimics the magnetic field, the curvature of current lines is not as pronounced as would be suggested by the field profile.

As the screening current bends around a corner into another quadrant the magnetic field is enhanced. This produces a region along the diagonal where the local field due to the supercurrent is greater and may screen the applied field more effectively. For small fields the magnetic flux is excluded along the diagonal but still penetrates from the middle of an edge.

If the field is then turned off to form a remnant state, the current must change directions to maintain the flux already trapped inside. The currents flowing close to the edge reverse directions so that the interior field of the film which was previously zero is still zero, while the trapped flux half way between the centre and the edge is maintained.

When the field was increased to a level shown by images in figure 5.5b (greater than 40 Oe), the applied field was strong enough to penetrate along the diagonals. When the field was turned off, currents changed directions throughout the sample and created a situation where shielding was largest along the diagonal. These regions maintained their trapped flux more efficiently and became local maxima. The diagonal maxima are shown as black crosses in figure 5.5b, while the diagonal minima are shown as light crosses in figure 5.5a (with the exception of the 30 Oe image).

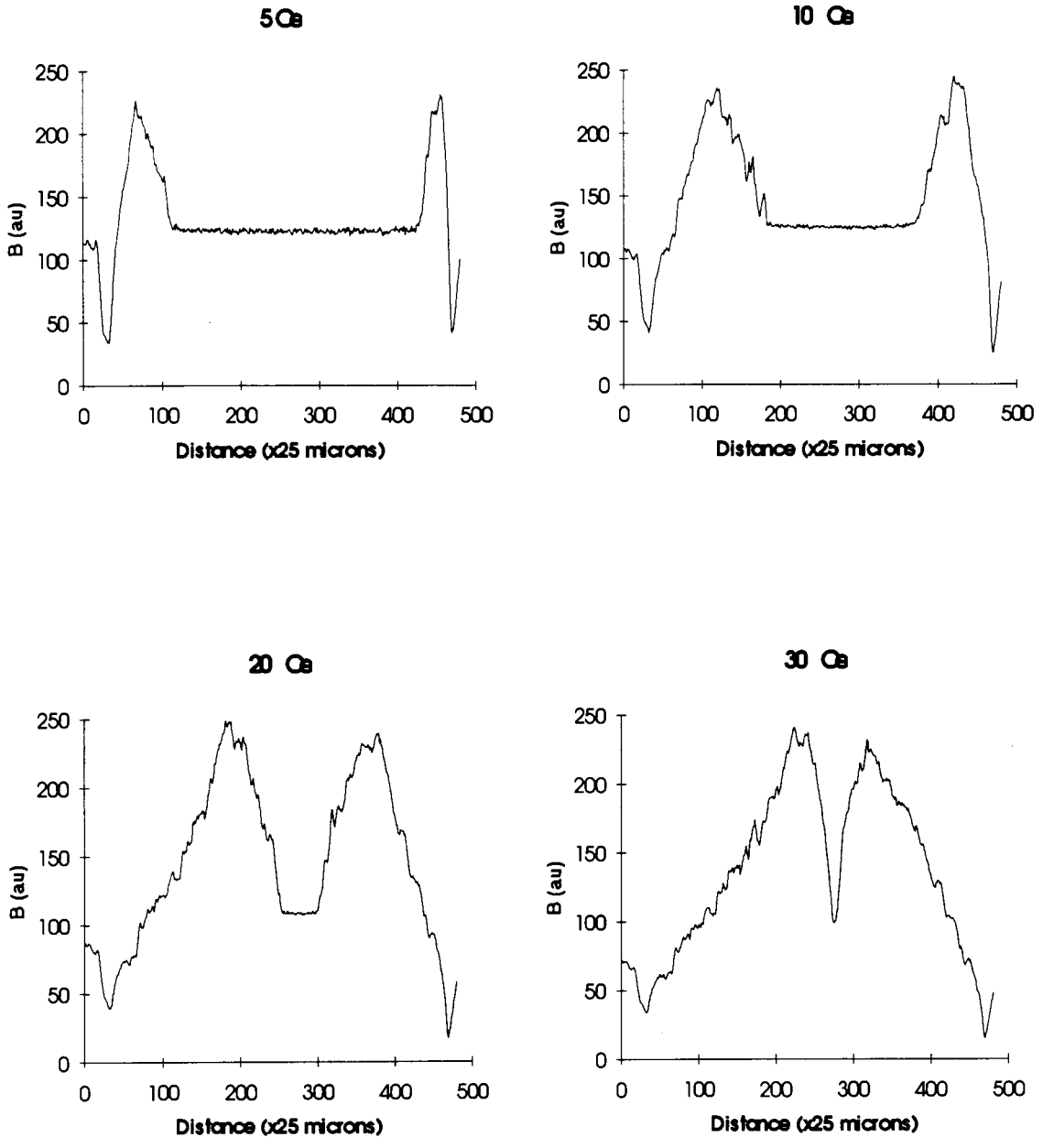

Figure 5.6a Cross sections of the magnetic field measured for a series of remnant states. The field has not been calibrated and is given in arbitrary units (au).

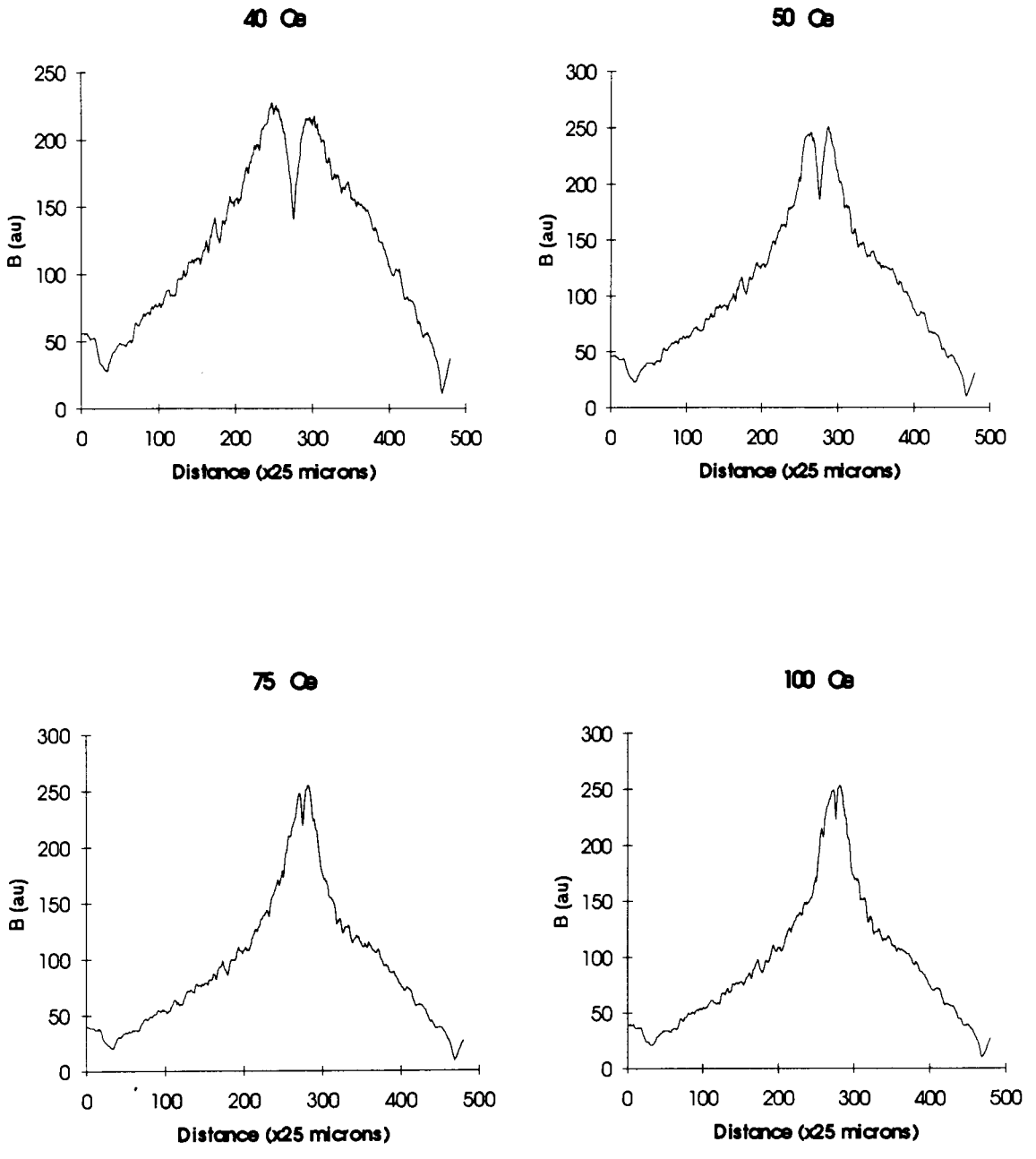

Figure 5.6b Cross sections of the magnetic field measured for a series of remnant states. The field has not been calibrated and is given in arbitrary units (au).

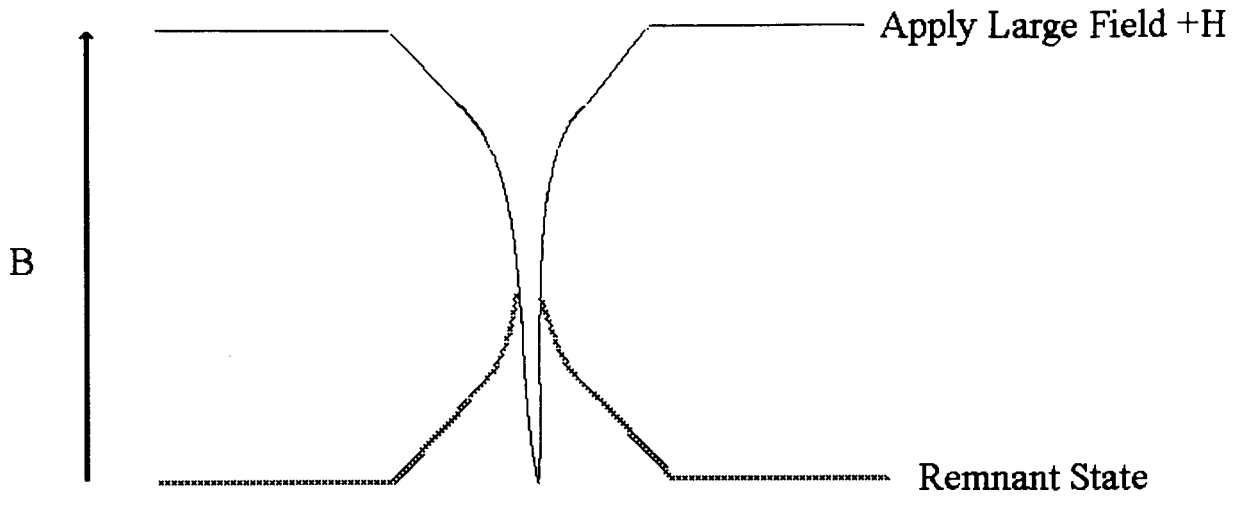

Figure 5.7 Remnant state after applying a high field.

Figure 5.6 shows a series of cross sections of the images shown in figure 5.5. A vertical slice was taken through the centre of the film and the magnetic field plotted against distance.

A change in the slope of B is evident towards the centre of the film at high fields (most noticeably in the 75 Oe and 100 Oe graphs) and a minimum intensity is observed at the peak of the pyramid at high fields. Figure 5.7 shows the field distribution responsible for the observed volcanoes. As square currents approach the centre of the film, they produce fields which are strong enough to cancel any large applied field for any value of J_C. There always exists a point in the centre of a thin film which is in a perfect Meissner state regardless of external conditions. The minimum collapsed to a size smaller than the garnet resolution under the influence of fields greater than 100 Oe. In a remnant state small current loops flowing around the centre must have opposite polarity to the screening currents throughout the sample in order to maintain the central minimum.

The magnetization plot is evidence that the observed symmetric flux pattern is due to geometric effects. The pattern reported by Huebener et. al.[9] (they used a Nb film and a EuS coating) suggested that the field in each of the four quadrants had an opposite polarity and that currents would flow alternately clockwise, and anti-clockwise. This result contradicts patterns observed in the present study.

These results were confirmed using a scanning Hall microprobe. The Hall probe was significantly further away from the surface (100 μm vs 10 μm) and had a much coarser resolution than the garnet film (25 μm vs 6 μm). Nevertheless, the scans correspond very well to those produced by the garnet film.

5.2 Critical Currents

Maxwell's equations state that $\nabla \times \mathbf{B} = \frac{4\pi}{c}\mathbf{J}$ and imply that the critical current density may be obtained by a suitable manipulation of the measured field distribution. If we restrict our attention to one side of the film and assume that the current flows parallel

to this side then we have $J_x = \frac{c}{4\pi}(\frac{\partial B_z}{\partial y} - \frac{\partial B_y}{\partial z})$. It was shown that the magnetic induction **B** which was measured just above the sample is equal to the magnetic induction inside the sample.

The low applied field data may be used to conveniently obtain critical current densities because these images contain two reference field regions i.e. the shielded region in the centre at 0 Gauss (assuming the ambient field to be negligible, in fact it is approximately 0.5 Gauss) and a distance outside the superconductor where the garnet indicates a field equal to the applied field. Assuming a linear response in the garnet, a number representing the field per pixel greyscale may be obtained. Figure 5.8 is a cross section of the previous sample in an applied field state. A value of 0.091 Gauss/intensity level was obtained.

A least squares fit was performed on the linear region close to the edge of figure 5.8 (between 80x25 microns and 100x25 microns on the graph). A slope of 27612 Gauss/m was obtained which gives a critical current of $27612\frac{Gauss}{m} \times \frac{1}{4\pi \times 10^{-3}} = 2.3 \times 10^2 \frac{A}{cm^2}$. This result is 3-4 orders of magnitude smaller than the expected value of J_C which is roughly 10^5-10^6 A/cm^2 . Baczewski et al.[28] performed a similar calculation on a disk shaped sample of $TmBa_2Cu_3O_{7-x}$ and found the calculation to be 3 orders of magnitude smaller than J_C (measured using a four point technique). It may be concluded that the extra term $\frac{\partial B_y}{\partial z}$ is more significant than $\frac{\partial B_z}{\partial y}$ in determining J_C. Daumlingand and Larbalestier[29] find that for a disk shaped superconductor the gradient of B_Z in the plane of the film is approximately

$$\frac{\partial B_z}{\partial r} = \frac{4\pi}{c} J_c \frac{d}{D} \qquad (11)$$

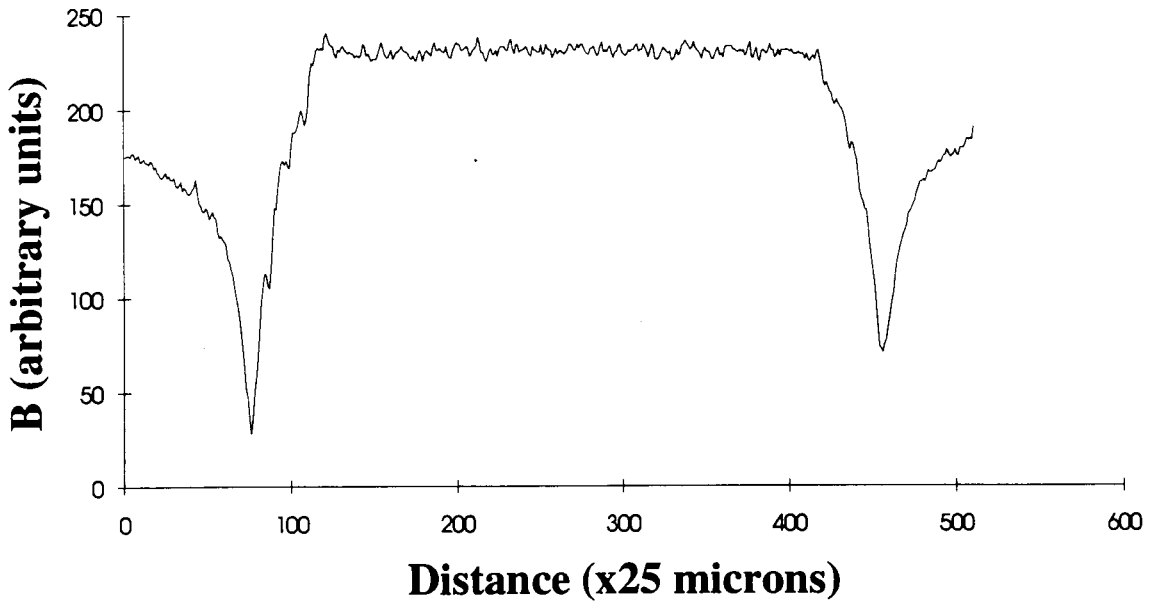

Figure 5.8 Cross section of field distribution of a thallium film in the presence of an applied field of 5 Oe. The magnetic induction of flat section in the centre is 0 Gauss, and B_z at the edge (distance=0 microns) is taken to be 5 Gauss.

where D is the diameter and d the thickness of the film. Naively applying this result to the present square sample and estimating D to be 1 cm and d as 1 μm the order of magnitude of J_C is then correct.

Maxwell's equation, $\nabla \times \mathbf{B} = \frac{4\pi}{c}\mathbf{J}$ immediately gives an estimate of the in-plane component of the magnetic field above the sample, by symmetry

$$\frac{\partial B_y}{\partial z} \approx \frac{2B_y}{d} \approx \frac{4\pi}{c} J_c \qquad (12)$$

5.3 Film Quality

The magneto-optical technique may be used to determine the quality of superconducting films on a macroscopic scale. The sample Y235 possess a large chip on one side. This chip acts as a vent for magnetic flux as may be seen in the sequence of images shown in figure 5.9.

As current flows along the edge it must divert around the chip thus producing a larger magnetic field on the inside of the loop driving the region 'normal'. The kink is unstable and will grow as the applied field is increased. A diagram showing the mechanism by which the kink propagates is shown in figure 5.10.

If a sample is cleaved on one side, many fine fragments of the film are chipped away, leaving a rough edge where flux may easily penetrate. The top edge of sample Y232B may be compared to the lower right edge in the images of figure 5.11. It is clear that this side has under-gone some sort of degradation process. An image of the largest chip on the top edge is shown in figure 5.12.

The camera lens was replaced with a microscope objective and images were taken of the flux penetrating through the defect. These images are shown in figure 5.13 (they

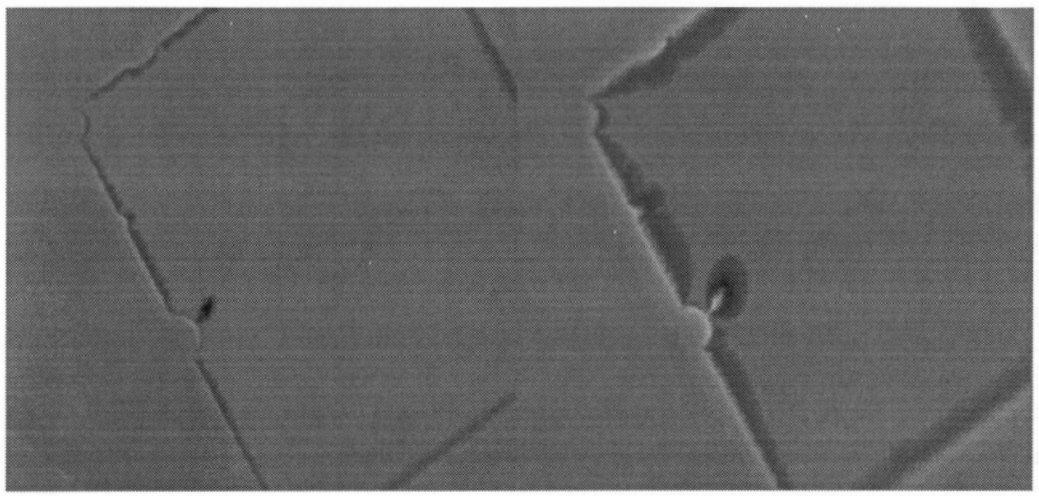

8 Oe 16 Oe

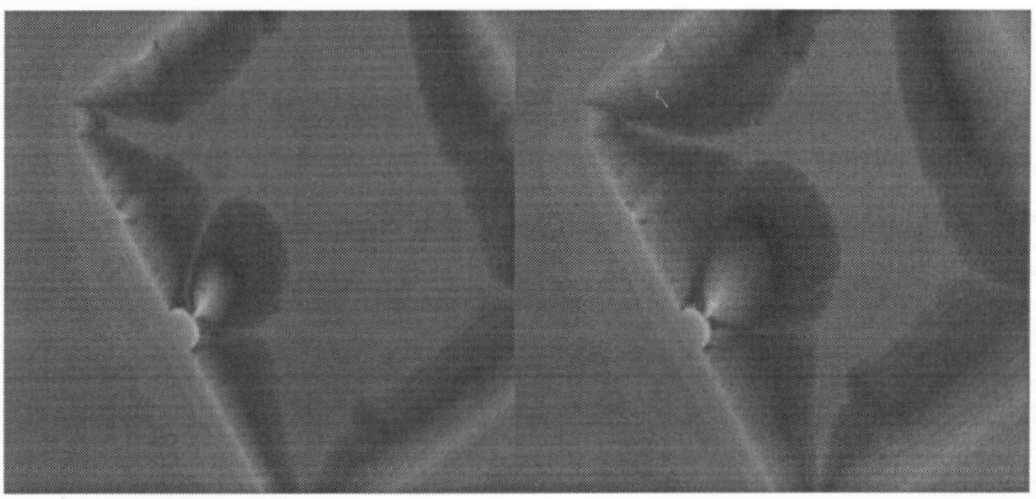

32 Oe 48 Oe

Figure 5.9 Series of images demonstrating the effect of an edge defect of the penetration of magnetic flux. The images are remnant states.

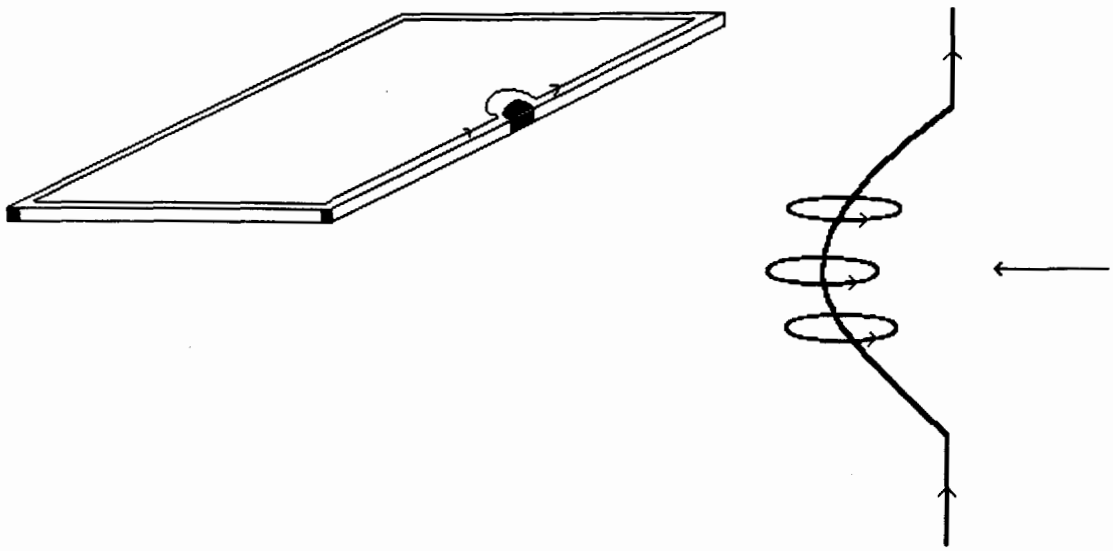

Figure 5.10 Currents divert around a small imperfection in film causing larger fields on the inside of the loop. The larger field is magnetically unstable and will tend to propagate further into the sample, this phenomenon is referred to as a kink instability.

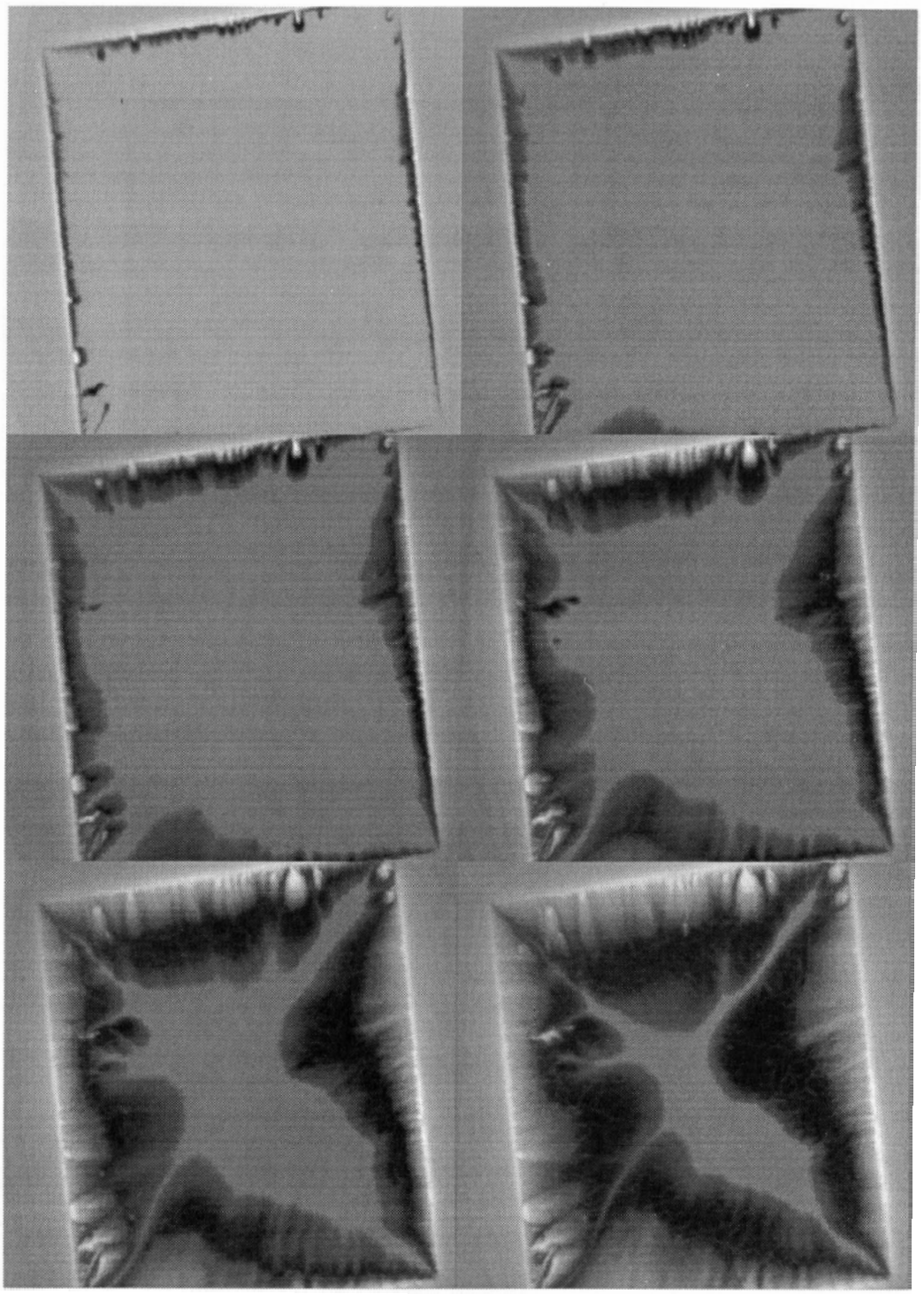

Figure 5.11 Series of images demonstrating the effect a poor edge has on flux penetration. The magnetic field is increasing from left to right and from top to bottom in the following sequence 16 Oe, 24 Oe, 32 Oe, 48 Oe, 72 Oe, 96 Oe

Figure 5.12 Chip on upper right corner of the sample.

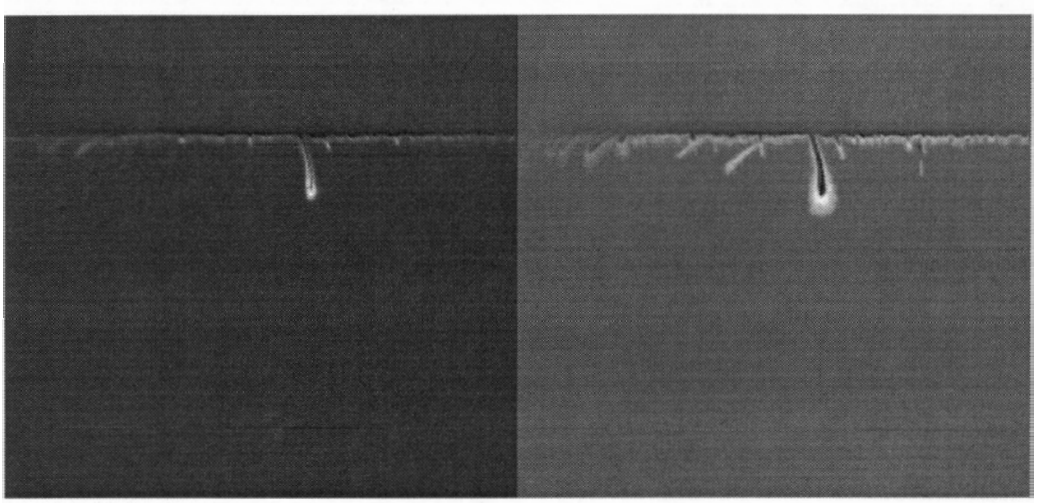

Figure 5.13a Series of images showing flux penetrating from a chip located on the edge of the film.

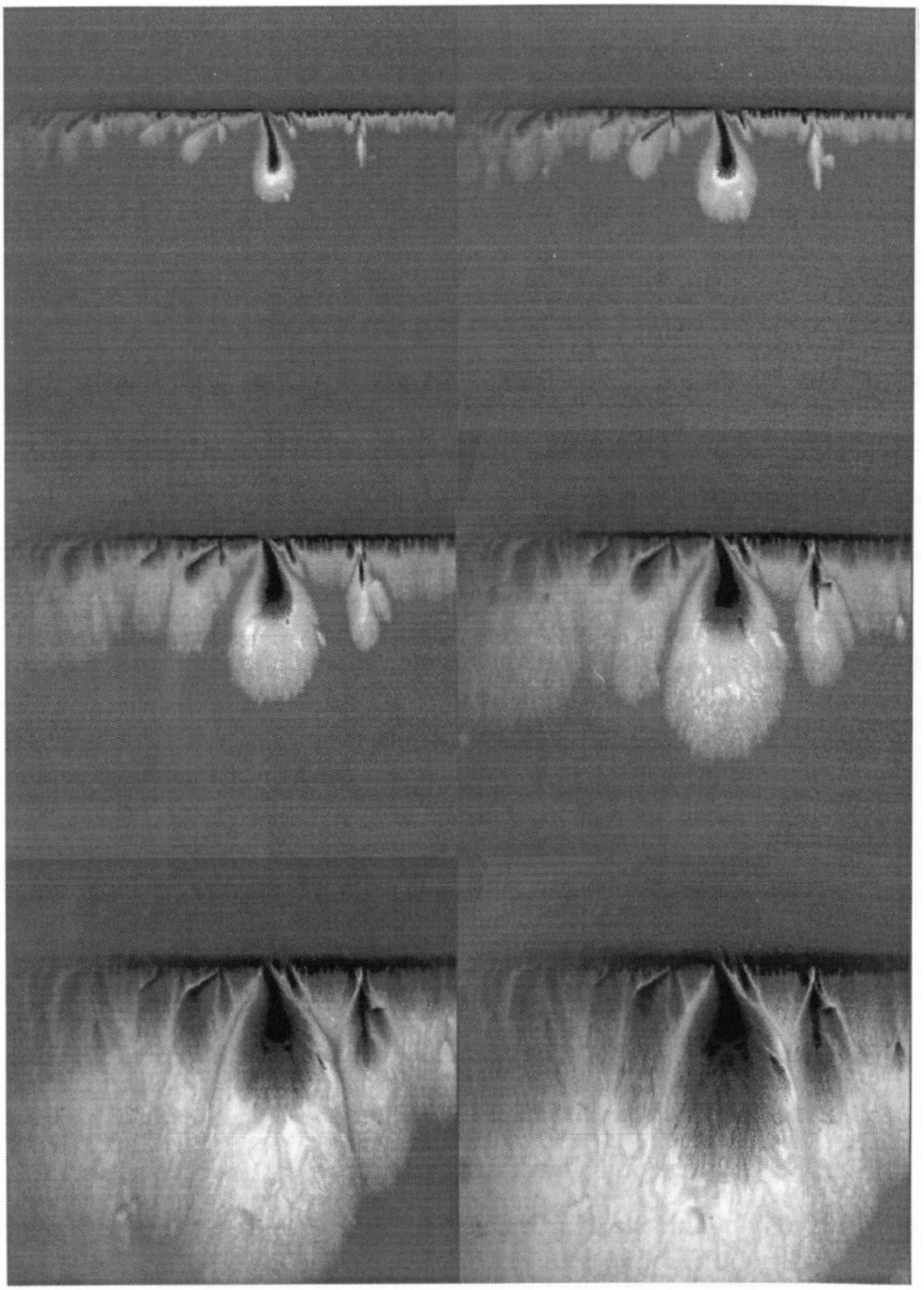

48 Oe 72 Oe

Figure 5.13b Series of images showing flux penetrating from a chip located on the edge of the film. The magnetic field is increasing from left to right and from top to bottom in the following sequence 12 Oe, 16 Oe, 24 Oe, 32 Oe, 48 Oe, 72 Oe

are approximately 1 x 1 mm). The defect is located on the right side of the top edge of the superconducting film.

A filamentary structure is seen in these images. This could either be a domain structure produced by the garnet film or preferential path by which flux moves in and out of the film.

Huebener and Kampwirth[30] reported seeing normal flux fingers penetrating into a strip of superconducting Indium using a magneto-optical technique and explain these fingers as kink instability in which a small diversion of current leads to the propagation of the normal region. The same effect may be occurring in the samples presented in this thesis, small microscopic defects (as opposed to large chips) might be causing small rivers of flux flow.

Besides detecting mechanical defects in films such as scratches and chips this technique may also probe chemical or environmental factors that might influence the superconducting state.

The thallium based film originally had a layer of photoresist approximately 25 μm thick on top (shown in figure 5.2 after photo-resist was removed). In order to get closer to the surface this layer was removed using spectro-grade acetone and deionized, distilled water. The film was then dried using nitrogen gas. A week later the film was re-examined and found to have been severely degraded. Several defects were evident on its surface and the trapped flux was observed to leak out at an accelerated rate. An image of the film after removal of the photoresist is shown in figure 5.14. The procedure to remove the photoresist is a standard procedure and should not adversely affect the superconductor. The observed deterioration of the film may be due to impurities in the deionized water or acetone.

To illustrate the effect of averaging the domain structure over a large number of trials the following images were taken of a DC SQUID under an applied field. The first image is a real picture of the DC SQUID under examination. The straight line running

down the centre of the DC SQUID is a step in the substrate used to form the weak links. The junction microbridge width was 15 μm. The second image shows the domain structure of the garnet under the influence of the DC SQUID in an applied field. The third image is the result of averaging 128 single images. The weak links could not be resolved.

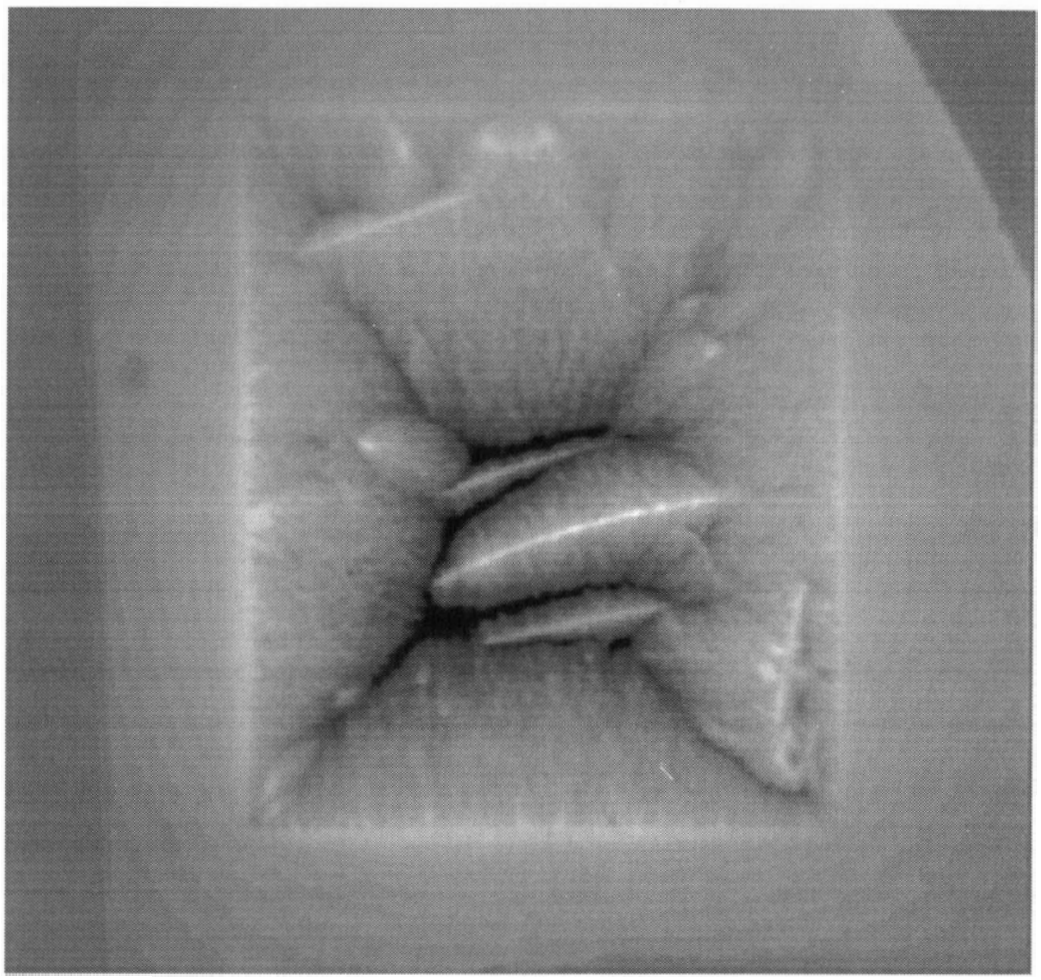

Figure 5.14 Image of thallium based film after layer of photo-resist had been removed. The film is in a remnant state after application of a large field (greater than 2H penetration).

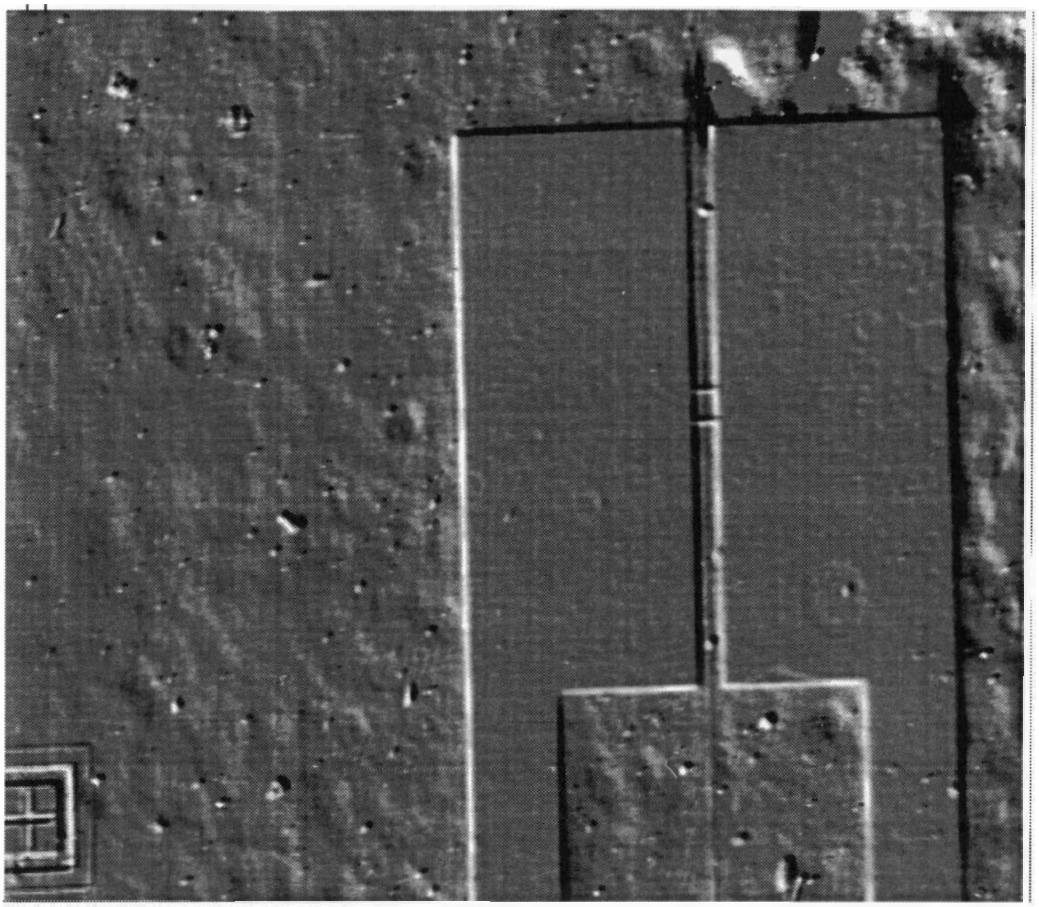

Figure 5.15 Real image of a DC SQUID. The superconducting pads are 8 mm x 8 mm.

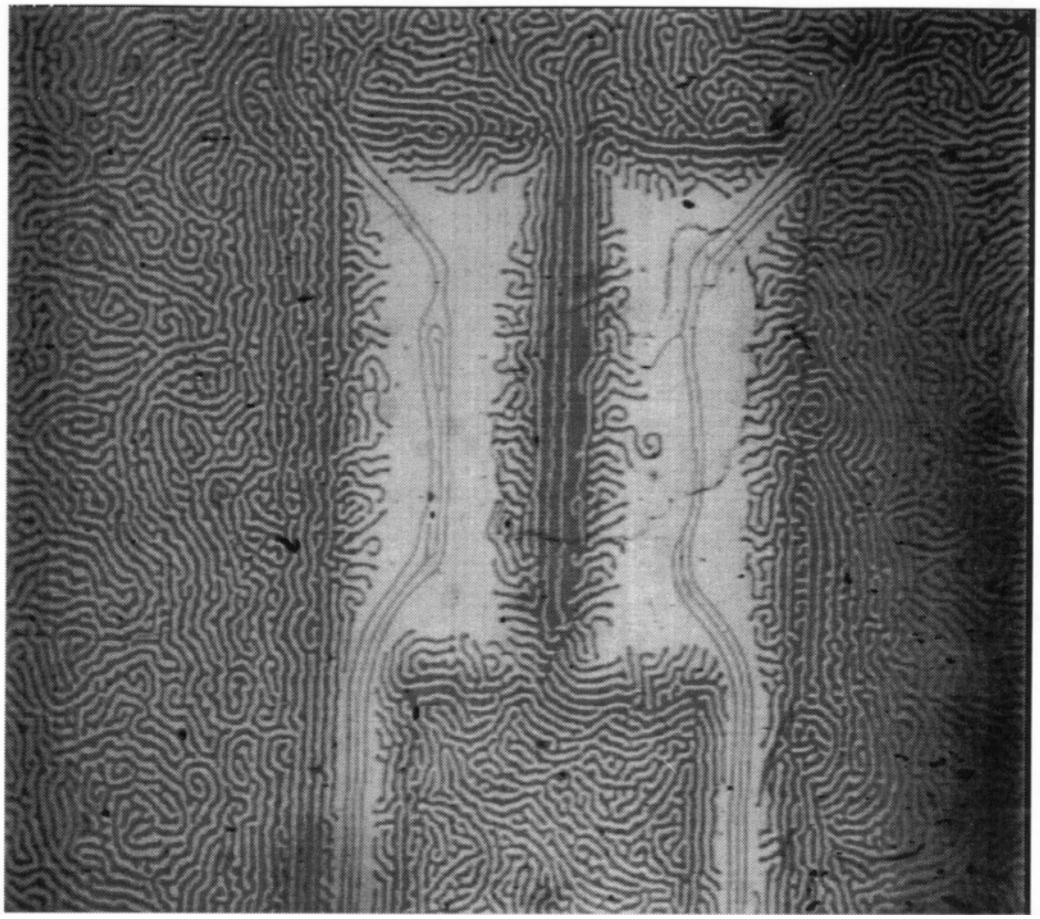

Figure 5.16 Single image of garnet domain structure due to the flux shielding of a DC SQUID. This is a remnant state after applying a 100 Oe field.

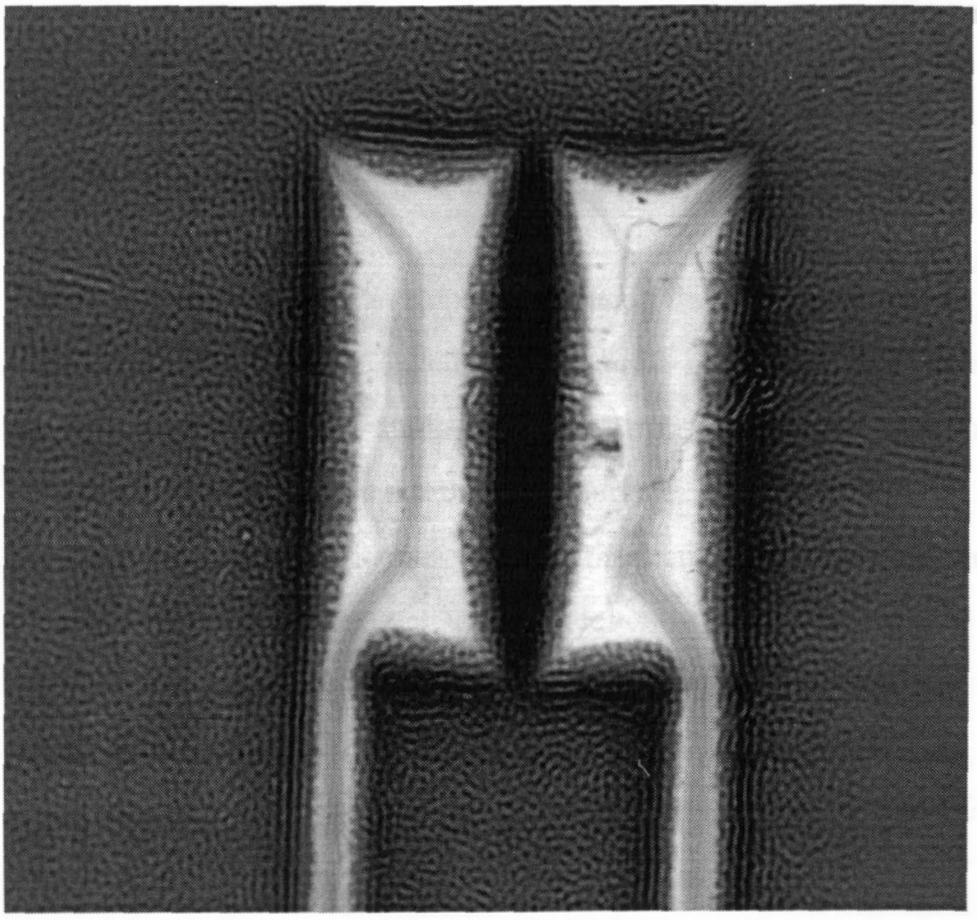

Figure 5.17 Average of 128 images of domain structure of garnet film under the influence of superconducting DC SQUID. This is a remnant state after applying a 100 Oe field. Dark areas around the DC SQUID edges are caused by demagnetization effects.

Chapter 6
Conclusion

6.1 Summary

A technique has been developed to map the magnetic field above a superconducting thin film using the Faraday effect and a magneto-optical garnet film in contact with the sample. Magnetic studies were performed on superconducting samples subjected to a magnetic field applied normal to the surface

Flux was observed to penetrate through the centre of a sample edge while shielding occurred along the diagonal. A theoretical current distribution based on Maxwell's equations was obtained using this data. This current distribution may be used to obtain estimates of the critical current of samples with arbitrary geometry. The data obtained in the present case have been used to calculate the current distributions in a square superconducting thin film.

The technique was used to illustrate the effect of various film defects on magnetic flux penetration into the interior of the sample. The results obtained were used to ascertain the quality of the films. These results were compared and verified qualitatively with a scanning Hall probe.

A DC SQUID was examined to determine whether one could resolve its weak links (nominally 15 μm wide). It was determined that the resolution afforded by the garnet film did not allow this to be accomplished.

6.2 Suggestions for Future Work

The technique developed here for magnetic field mapping may be used to provide feedback for quality control in the manufacture of superconducting thin films as it is inexpensive to develop and provides an effective, fast means of imaging film properties.

Given enhanced resolution the technique might eventually be used to image flux line dynamics in real time.

High resolution (≈20 μm) quantitative studies of current distributions should also be possible. The garnet film may be calibrated by obtaining hysteresis loops similar to figure 4.10. The sample would be warmed to a temperature above T_c, the hysteresis loops would then be acquired, the sample then cooled and data taken..

A new garnet film is being acquired which possesses an in-plane magnetization similar to the film used by Indenbom et. al.[31]. Polarized light will rotate according to how far the magnetization vector has been tilted towards the normal by an applied field. This film promises to have a greater resolution than the present garnet film as the domain structure perpendicular to the normal will be absent. Films of this nature do not have significant coercivity and have been reported to operate from 0 Oe up to 1000 Oe. This may be compared to a maximum of 20 Oe obtained with the present garnet film. The film does not have a domain structure perpendicular to the surface and therefore its lateral resolution is limited only by the anisotropic and exchange energies. It has been reported to have a resolution of 3 μm which will allow the examination of superconducting micro-structures such as weak links.

Appendix A

Example of Program to Acquire, Average and Display Data

Program Av_sub.C

```
#include <stdio.h>
#include <stdlib.h>
#include <dos.h>
#include<graphics.h>
#include<conio.h>
#include<alloc.h>
#include<math.h>
/*      This program is designed to control the Helmholtz coils through a digital to analog converter*/
/*      card located at port 736. It also uses a DOS program provided with the AVER2000 video card*/
/*      to save images on a virtual ram disk. The images are added sequentially and devided by a reference*/
/*      file if needed*/


/*      This program adds two images and then repeats a number times specified by the user    */
/*      Loop { H= h0; pause; H= h1; Get_Image; Add_it */
/*          H=-h0; pause; H=-h1; Get_Image; Add_it }  */
/*      it will then divide (if necessary) by a reference file.*/
/*      Images are obtained in some applied field with magnitude <Delta> specified by h0 and h1*/
/*      Input parameters: loop (unsigned char), h0(char), h1 (char) */
/*      and any_character_for_dividing  Exampel: av_add.exe 8 5 -3 any_c   */
/*      ( 8-loop; h0=5; h1=-3; and divide image by file D:\av_ref ) */

#ifdef __cplusplus
        int max(int value1, int value2);
        int max(int value1, int value2)
        {       return ( (value1 > value2) ? value1 : value2);      }
#endif
#ifdef __cplusplus
        int min(int value1, int value2);
        int min(int value1, int value2)
        {       return ( (value1 < value2) ? value1 : value2);      }
#endif


main(int argc,char **argv)    {

        FILE  *strea1,*strea2;

        char filenam1[10]="d:\\av";                          /* Image from AV2000*/
        char filenam2[15]="d:\\av_ref";                      /* File_Name_for_dividing*/
        char message[22]="Can't open file d:\\av";
        char h0,h1,ch[1];
        unsigned char row[640],loop;

        int loop_n,maxi,mini,mmi, driver=DETECT,mode;
        unsigned int i,j,k,x0,y0,ref[1280];
        unsigned long l,l0;
        int huge *image;

        float flti,maxf,minf,mmf;
```

```
loop=1;          h0=5;    h1=0;                    /* 20 Oe ?          */
if(argc>1)       loop=atoi(argv[1]);
if(argc>2)       h0=atoi(argv[2]);  if(h0>55) h0=0;
if(argc>3)       h1=atoi(argv[3]);  if(h1>55) h1=0;

outportb(0x737,128);       outportb(0x736,0);                    /* Zero H field          */
system("c:\\aver2000\\save.exe");                                /* Save 1 image D:\av    */
if((strea1=fopen(filenam1,"rb"))==NULL){printf("%s\n",message);return 1;}
fread(row,566,1,strea1);                                         /* Read Header of File   */
fclose(strea1);
x0=row[18]+256*row[19];   y0=row[22]+256*row[23];                /* Get Size of Image     */
l0=x0;   l0*=y0;                                                 /* l0 = file_size        */
         flti=l0;   printf("%g\n",flti);
if ((image=(int far *)farmalloc(2*l0))==NULL){printf("Can't allocate memory\n");return 1;}
for(l=0;l<l0;l++)   image[l]=0;
detectgraph(&driver,&mode);          initgraph(&driver,&mode,"c:\\borlandc\\bgi");
gotoxy(75,1);      printf("h0=%d\n",h0);                         /* print field 1   */
gotoxy(75,2);      printf("h1=%d\n",h1);                         /* print field 2   */
gotoxy(75,3);      printf("x=%d\n",x0);                          /* print max x   */
gotoxy(75,4);      printf("y=%d\n",y0);                          /* print max y   */
loop_n=0;
for(k=0;k<loop;k++){                                             /*Loop*/
        loop_n++;          if(loop_n>16)      loop_n=1;
        gotoxy(77,loop_n+5);        printf("%d",k);              /* print loop number */
        outportb(0x737,(128+h0));  outportb(0x736,0);            /* output to DAC H=+h0 */
        sound(40);         delay(234);        nosound();         /* Pause_Sound*/
        outportb(0x737,(128+h1));  outportb(0x736,0);            /* output to DAC H=+h1 */
        sound(100);        delay(44);         nosound();
        system("c:\\aver2000\\save.exe");                        /* Call DOS program to save 1 image as D:\av*/
        if((strea1=fopen(filenam1,"rb"))==NULL){printf("%s\n",message);return 1;}

        fread(row,566,1,strea1);                                 /* Bypass File_Header    */
        for(j=0;j<y0;j++) {                                      /*Add image to sum of previous images */
                l=j;       l*=x0;
                fread(row,x0,1,strea1);
                for(i=0;i<x0;i++)   image[i+l]+=row[i];}

        fclose(strea1);                                          /* end of + file */
        outportb(0x737,(128-h0));  outportb(0x736,0);            /* output to DAC H=-h0   */
        sound(40);         delay(234);        nosound();
        outportb(0x737,(128-h1));  outportb(0x736,0);            /* output to DAC H=-h1   */
        sound(100);        delay(44);         nosound();
        system("c:\\aver2000\\save.exe");                        /* Save  image D:\av     */
        if((strea1=fopen(filenam1,"rb"))==NULL){printf("%s\n",message);return 1;}
        fread(row,566,1,strea1);                                 /* Bypass File_Header    */
        for(j=0;j<y0;j++) {                  /* Subtract this image to sum of previous images */
                l=j;       l*=x0;
                fread(row,x0,1,strea1);
                for(i=0;i<x0;i++)   image[i+l]-=row[i];}
        fclose(strea1);}                                         /* end of - file */
                                                                 /*End of loop */

outportb(0x737,128);       outportb(0x736,0);                    /* Zero H field */

if(argc>4) goto div;                 /* Any 4-th parameter ? if so devide image by reference*/

maxi=-32767;       mini= 32767;
for(l=0;l<l0;l++){
        maxi=max(maxi,image[l]);
        mini=min(mini,image[l]);}
```

```
mmi=maxi-mini;
strea1=fopen("history","a");                                        /*append parameters of last operation into a
record file */
fprintf(strea1,"%d%s%d%s%d%s%d\n",loop," ",h0," ",h1," ",mmi);
fclose(strea1);
if((strea1=fopen(filenam1,"wb"))==NULL){printf("%s\n",message);return 1;}
for(j=0;j<y0;j++){                                                  /* scale image to 255 greyscale and display on sceen*/
        l=(y0-j-1);         l*=x0;
        for(i=0;i<x0;i++){
                flti=1.*(image[i+l]-mini)/mmi*255.;
                ch[0]=flti;
                fwrite(ch,1,1,strea1);
                putpixel(i,j,ch[0]/16);}}

goto end;

div:
        maxf=-32767;        minf= 32767;
        if((strea2=fopen(filenam2,"rb"))==NULL){printf("%s%s\n",message,"_ref");return 1;}
        for(j=0;j<y0;j++){
                l=(y0-j-1);         l*=x0;
                fread(ref,2*x0,1,strea2);
                for(i=0;i<x0;i++){
                        flti=1.*image[i+l]/ref[i];                  /* convert to floating point and devide by reference file*/
                        if(maxf<flti)       maxf=flti;
                        if(minf>flti)       minf=flti;}}

fclose(strea2);
mmf=maxf-minf;
strea1=fopen("history","a");
fprintf(strea1,"%d%s%d%s%d%s%g\n",loop," ",h0," ",h1," ",mmf);
fclose(strea1);
gotoxy(65,20);      printf("max=%f",maxf);
gotoxy(65,22);      printf("min=%f",minf);
if((strea1=fopen(filenam1,"wb"))==NULL){printf("%s\n",message);return 1;}
if((strea2=fopen(filenam2,"rb"))==NULL){printf("%s%s\n",message,"_ref");return 1;}
for(j=0;j<y0;j++){
        l=(y0-j-1);         l*=x0;
        fread(ref,2*x0,1,strea2);
        for(i=0;i<x0;i++)  {                                        /* scale image to 255 greyscale and display on screen  */
                flti=(1.*image[i+l]/ref[i]-minf)/mmf*255.;
                ch[0]=flti;
                fwrite(ch,1,1,strea1);
                putpixel(i,j,ch[0]/16);}}

end:

fcloseall();
sound(80);          delay(1000);        nosound();
closegraph();
farfree(image);
return 0;  }                                                        /*Main*/
```

References

(1) V.Z. Kresin, and S.A. Wolf, "Fundamentals of Superconductivity", Plenum Press, New York (1990).

(2) F. Weiss, J.P. Senatueur, A. Rouault, M. Audier, Y. Brechet, S. Blais, and R.Blum, *Cryogenics* **33**, 50 (1993).

(3) W. Xing, B. Heinrich, H.Zhou, A.A. Fife, and A.R.Cragg, "Magnetic Field Mapping, Magnetization, and Current Distributions of $YBa_2Cu_3O_7$ Thin Films by Scanning Hall Probe Measurements", to be published

(4) H. Ishigaki, M. Itoh, H. Endo, A. Hida, T. Yotsuya, and T.Minemoto, *Rev. Sci. Instrum.* **64**, 1049 (1993).

(5) E. Batalla, E. G. Zwartz, R. Goudreault, and L.S. Wright, *Rev. Sci. Instrum.* **61**, 2194 (1990).

E. Batalla, E.G. Zwartz, L.S. Wright, S.I. Raider,and A. Gupta, *Journal of Applied Physics* **69**, 7178 (1991).

E. Batalla, E.G. Zwartz, L.S. Wright, P.D. Grant, and M.W. Denhoff, *Can. J. Phys.* **69**, 786 (1991).

(6) M.R. Koblischka, N. Moser, B. Gegenheimer, and H. Kronmuller, *Physica C* **166**, 36 (1990).

A. Forkl, H. Habermeier, B. Leibold, T. Dragon, and H.Kronmuller, *Physica C* **180**, 155 (1991).

A. Forkl, T. Dragon, H. Kronmuller, H.U. Habermeier, G. Mertens, *Applied Physics Letters* **57**, 1067 (1990).

(7) M.V. Indenbom, V.I. Nikitenko, A.A. Polyanskii and V.K. Vlasko-Vlasov, *Cryogenics* **30**, 747 (1990).

S.Goto, *ISTEC Journal* **3**, 44 (1990).

(8) P. Laeng, and L.Rinderer, *Cryogenics* **8**, 315 (1972).

(9) R.P Huebener, V.A. Rowe, R.T. Kampwirth, *Journal of Applied Physics* **41**, 2963 (1970).

(10) C.A. Duran, P.L. Gammel, R. Wolfe, V.J. Fratello, D.J. Bishop, J.P. Rice, and D.M.Ginsberg, *Nature* **357**, 474 (1992).

(11) M. Turchinskaya, D.L. Kaiser, F.W. Gayle, A.J. Shapiro, A. Roytburd, V. Vlasko-Vlasov, A. Polyanskii, and V. Nikitenko, *Physica C* **216**, 205 (1993).

(12) V.K. Vlasko-Vlasov, L.A. Dorosinskii, M.V. Indenbom, V.I. Nikitenko, A.A. Polyanskii, A.V. Antonov, Yu.M. Gusev, and G.A. Emelchenko, *Superconductivity* **4**, 1007 (1991).

(13) A.H. Bobeck, and E.D. Torre, " Magnetic Bubbles", North Holland Publishing Company, New York (1975).

(14) T.H. ODell, "Magnetic Bubbles", John Wiley and Sons, New York (1974).

(15) K. Matsumoto, S. Sasaki, K. Haraga, K. Yamaguchi, and T Fujii, *IEEE Transactions on Magnetics* **28**, 2985 (1992).

(16) H. Jouve, "Magnetic Bubbles", Academic Press, Orlando (1986).

(17) H. Dotsch, P.Hertel, B. Luhrmann, S. Sure, H.P. Winkler, and M. Ye, *IEEE Transactions on Magnetics* **28**, 2979 (1992).

(18) R. Carey, and E.D. Isaac, "Magnetic Domains and Techniques for their Observation", Academic Press, New York (1966).

(19) A.H. Eschenfelder, "Magnetic Bubble Technology", Springer-Verlag, New York (1981).

(20) T.P. Orlando, and K.A. Delin, "Foundations of Applied Superconductivity" , Addison-Wesley Publishing Company, Reading Massachusetts (1991).

(21) V.L. Newhouse, "Applied Superconductivity", John Wiley and Sons Inc., New York (1964).

(22) D. Shoenberg, "Superconductivity", Cambridge University Press, Cambridge (1962).
Shu-Ang Zhou, "Electrodynamic Theory of Superconductors", Peter Peregrinus Ltd., London (1991).

(23) J. Bardeen, L.Cooper, J. Schrieffer, *Physical Review* **108**, 1175 (1957).

(24) M. Crisan, "Theory of Superconductivity", World Scientific Publishing Co., New Jersey (1989).

(25) C.P. Bean, *Reviews of Moderm Physics* **36**, 31 (1964).

(26) Y.B. Kim, C.F. Hempstead, and A.R. Strnad, *Physical Review* **129**, 528 (1963).

(27) P. Brull, D. Kirchgassner, and P. Leiderer, *Physica C* **182**, 339 (1991).

(28) L.T. Baczewski , K. Piotrowski, R Szymczak, H Szymczak, and A.P. Malozemoff, *Physica C* **175**, 363 (1991).

(29) M. Daumling, and D.C. Larbalestier, *Physical Review B* **40**, 9350 (1989).

(30) R.P. Huebener and R.T. Kampwirth, *Phys. Stat. Sol.* **13**, 255 (1972).

(31) M.V. Indenbom, Th. Scuster, M.R. Koblischka, A. Forkl, H. Kronmuller, L.A. Dorosinskii, V.K. Vlasko-Vlasov, A.A. Polyanskii, R.L. Prozoorov and V.I. Nikitenko, *Physica C* **209**, 259 (1993).